Applied Geochemistry 75 (2016) 171–188

Contents lists available at ScienceDirect

Applied Geochemistry

journal homepage: www.elsevier.com/locate/apgeochem

Compositional multivariate statistical analysis of thermal groundwater provenance: A hydrogeochemical case study from Ireland

Sarah Blake [a, b, *], Tiernan Henry [b], John Murray [b], Rory Flood [c], Mark R. Muller [d], Alan G. Jones [a], Volker Rath [a]

[a] Dublin Institute for Advanced Studies, Ireland
[b] Earth and Ocean Sciences, National University of Ireland, Galway, Ireland
[c] School of Geography, Archaeology and Palaeoecology, Queen's University Belfast, UK
[d] Independent Geophysical Consultant, Cambridge, UK

ARTICLE INFO

Article history:
Received 18 November 2015
Received in revised form
11 May 2016
Accepted 17 May 2016
Available online 19 May 2016

Keywords:
Hydrochemistry
Compositional data analysis
Principal component analysis
Low-enthalpy geothermal
Thermal springs
Ireland

ABSTRACT

Thermal groundwater is currently being exploited for district-scale heating in many locations worldwide. The chemical compositions of these thermal waters reflect the provenance and circulation patterns of the groundwater, which are controlled by recharge, rock type and geological structure. Exploring the provenance of these waters using multivariate statistical analysis (MSA) techniques increases our understanding of the hydrothermal circulation systems, and provides a reliable tool for assessing these resources.

Hydrochemical data from thermal springs situated in the Carboniferous Dublin Basin in east-central Ireland were explored using MSA, including hierarchical cluster analysis (HCA) and principal component analysis (PCA), to investigate the source aquifers of the thermal groundwaters. To take into account the compositional nature of the hydrochemical data, compositional data analysis (CoDa) techniques were used to process the data prior to the MSA.

The results of the MSA were examined alongside detailed time-lapse temperature measurements from several of the springs, and indicate the influence of three important hydrogeological processes on the hydrochemistry of the thermal waters: 1) salinity and increased water-rock interaction; 2) dissolution of carbonates; and 3) dissolution of sulfides, sulfates and oxides associated with mineral deposits. The use of MSA within the CoDa framework identified subtle temporal variations in the hydrochemistry of the thermal springs, which could not be identified with more traditional graphing methods, or with a standard statistical approach. The MSA was successful in distinguishing different geological settings and different annual behaviours within the group of springs. This study demonstrates the usefulness of the application of MSA within the CoDa framework in order to better understand the underlying controlling processes governing the hydrochemistry of a group of thermal springs in a low-enthalpy setting.

1. Introduction

Deep, thermal groundwater is currently being exploited for district-scale heating in many locations world-wide, such as Paris, France (Castillo et al., 2011), Milan, Italy (Sparacino et al., 2007), and Southampton, United Kingdom (Busby, 2010). It is now being explored in Ireland as part of the IRETHERM project, one aim of which is to determine the suitability of Irish thermal springs as a geothermal energy resource. The hydrochemical signatures of the thermal springs are indicative of a meteoric origin (Burdon, 1983; Mooney et al., 2010); given this hydrochemistry and their elevated temperatures, the thermal springs are expected to comprise a mixture of groundwaters from different sources and different recharge areas. Understanding the interactions of these hydrochemical elements is critical for characterising the springs as a geothermal energy resource.

* Corresponding author. Dublin Institute for Advanced Studies, 5 Merrion Square, Dublin 2, Ireland.
E-mail address: sblake@cp.dias.ie (S. Blake).

http://dx.doi.org/10.1016/j.apgeochem.2016.05.008
0883-2927/

In Ireland, average groundwater temperatures typically range from 9.5 to 10.5 °C (Aldwell and Burdon, 1980). As defined by Aldwell and Burdon (1980), thermal springs are considered to be those natural groundwater springs where the mean annual temperature is appreciably warmer than average groundwater temperatures. In this study springs with a mean annual temperature above 12 °C are considered thermal. Forty-two thermal springs and thermal shallow groundwater occurrences have been recorded to date in Ireland (Goodman et al., 2004) (Fig. 1c)). These springs range in temperature up to 25 °C, and three have maxima in excess of 20 °C. Some of the springs have been utilised in the past as therapeutic spa wells (e.g., Lady's Well, Mallow, Co. Cork (average temperature of 19.5 °C); Louisa Bridge Spa Well, Leixlip, Co. Kildare (maximum of 17.5 °C)), and many more have religious and cultural significance, as holy wells, as is evident from their names (e.g., St. Brigid's Well, Co. Dublin (maximum of 19 °C); St. Gorman's Well, Co. Meath (maximum of 21.8 °C)). The thermal spring waters at Lady's Well in Mallow have been used to partially heat a municipal swimming pool (Goodman et al., 2004). To date, this is the only recorded example of an Irish thermal spring being utilised as a source of geothermal energy.

The multi-disciplinary IRETHERM investigation of Irish thermal springs aims to (1) identify the source aquifer(s) for the thermal waters, (2) characterise the circulatory system, and (3) assess the potential for the existence of deeper, higher-temperature circulation patterns for future geothermal exploitation. In this paper, new hydrochemical data from a small sub-set of the thermal springs are analysed using a compositional data analysis (CoDa) approach to multivariate statistical analysis (MSA), and interpreted alongside high-resolution, time-lapse temperature and electrical conductivity measurements to better characterise the source of the thermal waters.

Six springs in the Carboniferous Dublin Basin, in the east-central region of Ireland, were selected for detailed investigation (Fig. 1c)). These springs were chosen for both their proximity to urban centres, which could make them suitable for geothermal use, and for their individual hydrogeological attributes. The results presented here represent the first detailed exploratory statistical analysis of hydrochemical data from these thermal springs. The chemical composition of groundwater frequently reflects the chemical composition of the host bedrock, and can provide valuable information on inputs to the hydrogeological system that further influence the hydrochemistry (Güler et al., 2012). Hydrochemical analysis is especially useful in karstified areas, where hydrochemical data is often equally or more important than traditional hydrodynamic data when attempting to understand and model groundwater flow (Pavlovskiy and Selle, 2015). King et al. (2014) noted that studies focusing on the groundwater chemistry to assess interactions between different types of groundwater were only useful if their chemistries were sufficiently different. Similar observations have led to the increasing use of more objective, discriminative approaches, such as MSA, which can identify subtleties and complexities that are often overlooked by more traditional methods of analysis (e.g., Cloutier et al., 2008; Page et al., 2012; Raiber et al., 2012; Daughney et al., 2012; Menció et al., 2012; Hu et al., 2013; Engle and Rowan, 2014; Giménez-Forcada and Vega-Alegre, 2015).

Hydrochemical data from a single sample consist of a series of measurements of analytes, commonly expressed in proportions such as mg/L, ppm or ppb. A change in one component of the solution modifies the relative amount of every other component; the data are compositional. Problems can arise when standard statistical tools are applied to investigate compositional data unless the data are properly processed beforehand. In the Supplementary material of this paper, we show how the application of CoDa techniques to the data prior to the MSA results in a more realistic and insightful analysis, as compared to a more standard statistical analysis of the data. A compositional approach to MSA is used here to: 1) highlight differences in the hydrochemistry within the dataset; 2) distinguish between the thermal springs and typical cold groundwater in the area; and 3) shed light on the temporal variation in the behaviour of the springs.

2. Study area in context

2.1. Geological setting of the Irish thermal springs

The Irish thermal springs occur in Carboniferous limestones along a wide northeast (NE) to southwest (SW) lineament that traverses the centre of Ireland, and is broadly coincident with the putative trend of the Iapetus Suture Zone (ISZ) (Fig. 1a)). The ISZ is a major tectonic structure in Irish geology and separates two former continents, Laurentia and Avalonia, which converged during the Caledonian orogenic cycle approximately 475 to 405 Ma (e.g., Chew, 2012). Terrestrial, red-bed, clastic facies were deposited on the resulting landmass during the Devonian period (e.g., Graham, 2009), followed by a shift to predominantly carbonate deposition as a result of a regional marine transgression during earliest Carboniferous times (MacDermot and Sevastopulo, 1972). Extensive carbonate production continued in Ireland for much of the Mississippian epoch (e.g., Somerville, 2008), which was followed by a switch to non-calcareous facies during the upper Mississippian and lower Pennsylvanian epochs (e.g., Fallon and Murray, 2015).

The Carboniferous (Mississippian: Tournaisian to Viséan) limestones that host the thermal springs tend to exhibit low primary porosity. Permeability is greatly improved by karst and fracture development, which provide important conduits and fissures for groundwater flow. The thermal springs are frequently associated with deep-seated, high-angle faults, which transport the warm waters to the surface (Mooney et al., 2010). The Carboniferous limestones in the Irish Midlands are also host to significant (world-class) massive sulfide deposits (Wilkinson and Hitzman, 2015). These mineral deposits also have a close spatial relationship with the ISZ (Fig. 1a)), and their extensive development attests to the operation of very large hydrothermal systems in the past (Wilkinson, 2010). Both the thermal springs and the mineral deposits are associated with dominant NE-SW structural lineaments. These deep-seated, pervasive faults, although no longer active, may still provide fluid pathways enhanced by dissolutional processes in places (karstification), allowing water to flow from deeper units up to the surface, and are probably very important in controlling regional groundwater flow (Henry, 2014).

The six springs chosen for further study are situated in the Carboniferous Dublin Basin, which contains c. 2000 m of sedimentary infill. During the Viséan age, active faulting within the basin led to the development of shallow platforms and contrasting deeper regions. The platform facies are typically clean, thickly bedded, and shale-free limestones, whereas the deeper basinal facies are thinly inter-bedded, cherty limestones and shales (mapped regionally as the Lucan Formation or 'Calp'; see Marchant and Sevastopulo, 1980). The interface between the initial phase of ramp sedimentation and subsequent development of shelf platforms in the Dublin Basin is marked by a widespread phase of Waulsortian carbonate mudbank ('reef') development (Lees and Miller, 1995). Four out of the six thermal springs studies here discharge from mapped Waulsortian limestone localities. These fine-grained limestones commonly contain infilled, sparry cavities and are quite pure (in terms of carbonate content), which makes them susceptible to karstification. These mudbanks commonly formed aggregates with intervening, laterally equivalent, off-bank

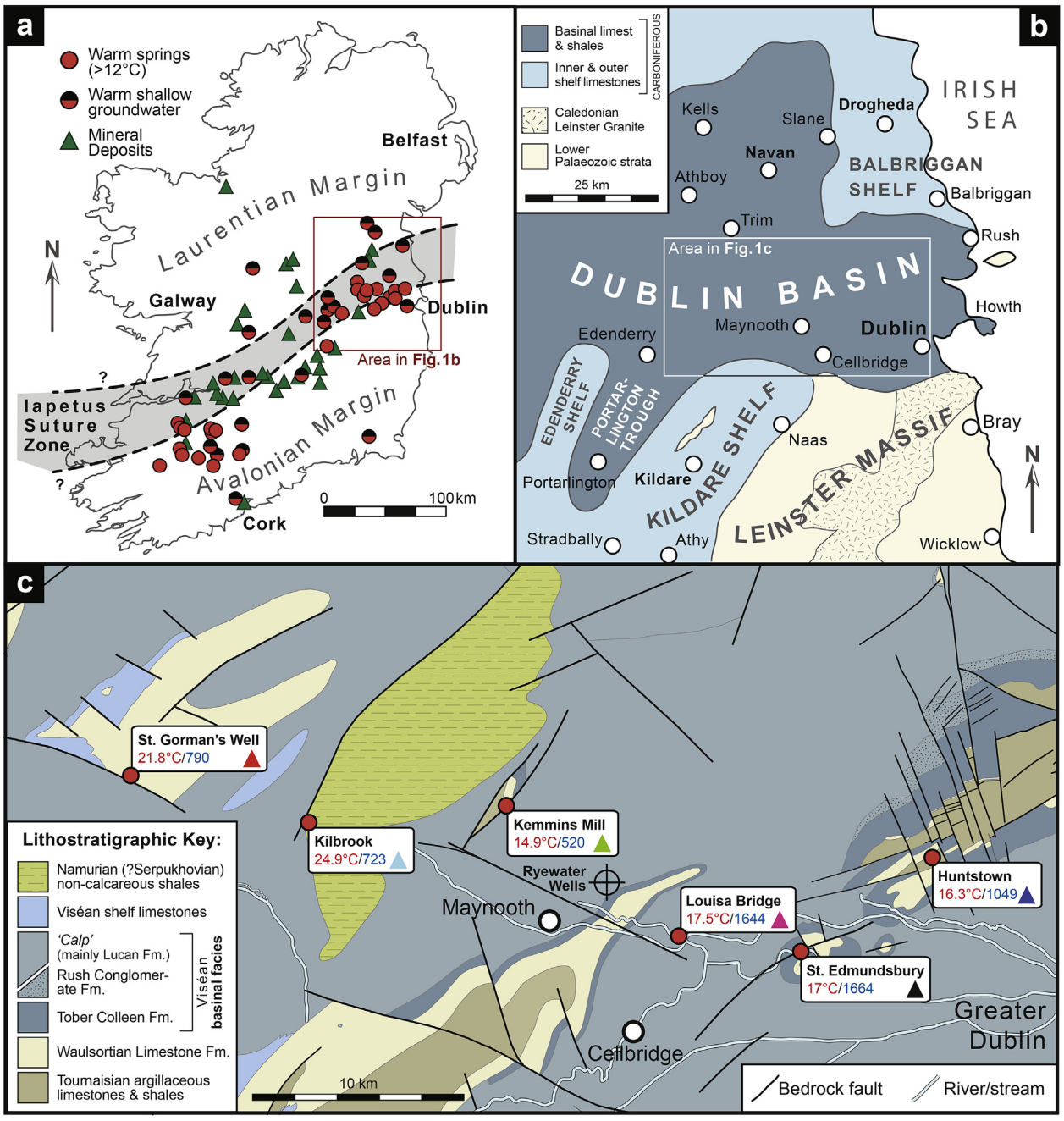

Fig. 1. Location and geological setting of Irish thermal groundwaters: (a) general location of Irish thermal spring and thermal shallow groundwater locations (after Goodman et al., 2004) along with mineral deposits and the approximate trace of the Iapetus Suture Zone (after Wilkinson, 2010); (b) generalised palaeogeographic map of the Dublin Basin during the Viséan Stage (modified from Sevastopulo and Wyse Jackson (2009)); and (c) detailed geological map of the study area, within the Carboniferous Dublin Basin, showing thermal springs included in the hydrochemical sampling programme (red circles), and the location of the Ryewater monitoring wells. The maximum temperature (red) and electrical conductivity in μS/cm (blue) are given for each thermal spring (data from HOBO loggers). Coloured triangles in each of the thermal spring labels refer to colour coding used for these locations in subsequent figures. Geology map from the Geological Survey of Ireland (www.gsi.ie).

facies, which are typically represented by thin, nodular, chert-rich shales. The thickest developments of Waulsortian limestones in the Dublin Basin are over 500 m thick (Strogen et al., 1996), and it is highly likely that deep faults in this lithology play an important role in facilitating the ascent of the thermal spring waters to the surface.

2.2. Hydrogeological setting

The thermal springs studied in this work are situated in a relatively flat and low-lying landscape, predominantly used for agricultural purposes, in the eastern part of Ireland. The spring elevations range from approximately 20 to 90 m above ordnance datum. The 30-year (1981–2010) average annual rainfall in the area is 868 mm/yr (Walsh, 2012) and evaporative losses for the region are estimated at 450 mm/yr (Met Éireann). The bedrock of the study area is broadly classified by the Geological Survey of Ireland (GSI) as "locally important, moderately productive" limestone aquifer. Most recharge to aquifers in Ireland occurs in the period

Table 1
Morphological and geological setting of the Leinster thermal springs and cold seepages surveyed in this study. Temperature data for the two cold seepages measured with a Hanna Combo meter. Other temperature data measured by HOBO temperature loggers.

Spring	Location	Geological setting	Max. T (°C)	Description
St. Edmundsbury spring	53°21′58.59″N 6°25′35.42″W	Waulsortian Limestone Fm.	17.0	Discharges from bedrock on south bank of River Liffey. Flooded periodically (minimum temperature not representative of thermal groundwater). Conspicuous iron staining from spring waters.
St. Gorman's Well	53°26′34.57″N 6°53′9.68″W	Adjacent to faulted contact between Waulsortian Limestone Fm. and Lucan Fm.	21.8	Ephemeral pond, adjacent borehole used for sampling – drilled in 1980s. Normal flow pattern is artesian in winter (max. ~ 1000 m^3/d) when pond is full. Maximum temperatures in winter.
Huntstown Fault spring	53°24′11.44″N 6°19′54.29″W	Strike-slip fault of Cenozoic age in Boston Hill Fm. limestone	16.3	Discharges from 1 m wide cavity along fault. Steady temperature and maximum discharges of ~5000 m^3/d reported.
Kemmins Mill spring	53°25′47.13″N 6°38′35.16″W	Gravelly till deposits overlying faulted contact between Lucan Fm. and older limestones	14.9	Shallow abstraction well in gravel deposits used for domestic and farming purposes. Steady temperature and "slow boil" bubbling.
Kilbrook spring	53°25′24.23″N 6°46′31.63″W	Gravel and sand glacial till over faulted contact between Lucan Fm. and younger Namurian deposits	25.0	Discharges from old gravel quarry excavations. Depth to bedrock estimated at 25–30 m. Discharge (max. ~ 850 m^3/d) greatest in winter. Fairly steady, high temperature throughout the year.
Louisa Bridge Spa Well	53°22′14.44″N 6°30′23.42″W	Gravel deposits overlying Lucan Fm. limestone	17.5	Historical spa well and pond with engineered surrounds built in early-19th century. Steady temperature, yellowish-orange deposits left by spring water.

between October and April, and typical estimated recharge rates for this area are 101–200 mm/yr (Hunter Williams et al., 2011). The thermal springs surveyed in this study generally have their maximum discharges in the winter, when recharge rates are highest. Where known, these discharge values are presented in Table 1. No detailed hydrodynamic data was available for this study.

The hydrochemical signatures of Irish thermal springs imply that they are mainly composed of meteoric waters that are recently recharged from rainfall events (Burdon, 1983; Mooney et al., 2010). For a better interpretation, the results of the hydrochemical analysis of the thermal spring waters are compared here with observations from "typical" Irish carbonate groundwaters. Fig. 2 is a (non-compositional) Piper diagram comparing the six thermal springs and two cold seepages from this study with historical monitoring well data collected by the Irish Environmental Protection Agency (EPA) at Ryewater between 2009 and 2012 (the location of the Ryewater sampling points can be seen in Fig. 1c), and information about the installations is provided in the Supplementary material). Fig. 2 shows that most of the thermal springs have major ion compositions that are comparable to Irish carbonate groundwaters ($CaHCO_3$-type).

As noted by Burdon (1983), there are hydrochemical traits in some of the thermal springs that, along with their elevated temperatures, suggest longer residence times and deeper circulation patterns (e.g., the high electrical conductivities seen in St. Edmundsbury spring and Louisa Bridge Spa Well in Table 3). Dissolved inert gas and isotopic analyses carried out by Burdon (1983) suggest that Louisa Bridge Spa Well has a component of water with a residence time in excess of 30,000 years. Thus, water samples recovered from the Leinster thermal springs are likely to be a mixture of groundwaters from different sources and different recharge areas (e.g., a thermal spring water could be composed of a mixture of deeper-circulating, older groundwater, and more recent recharge from a shallow groundwater system).

3. Materials and methods

3.1. Sample collection and analysis

New samples from six thermal springs (Fig. 1c)) and two cold seepages are the focus of this study. Geographical coordinates, geological setting, temperature range and a brief description of each spring is provided in Table 1. Data were recovered for analysis over five seasons to assess the temporal variation in the spring chemistry and to provide some seasonal overlap for a more robust analysis. The springs were sampled in July/August and October 2013, and in January, May and August 2014. Samples were not collected from St. Edmundsbury spring in January 2014 as the spring was flooded by the River Liffey at that time. Each sample was duplicated, i.e., there are ten samples for each sampling point collected at five different times (with the exception of St. Edmundsbury spring, which has eight samples collected over four seasons). Temperature (°C) and electrical conductivity (μS/cm) were recorded at each spring prior to sampling using a calibrated YSI 556 portable multi-probe. The pH was recorded using a Hanna HI 98130 Combo meter (use of both instruments facilitated cross-checking of results).

A total of 78 water samples (not including blanks) were analysed for major and minor ions by ELS Ltd., Cork, Ireland, and also for a suite of 70 trace elements by Acme Ltd. (now trading as Bureau Veritas Ltd.), Vancouver, Canada. Further details of the sampling protocol and laboratory analysis are provided in the Supplementary material. Table 2 presents details of the analytes retained for the final analysis, including limits of quantification (LOQ) and the percentage of observations below the LOQ for each sample.

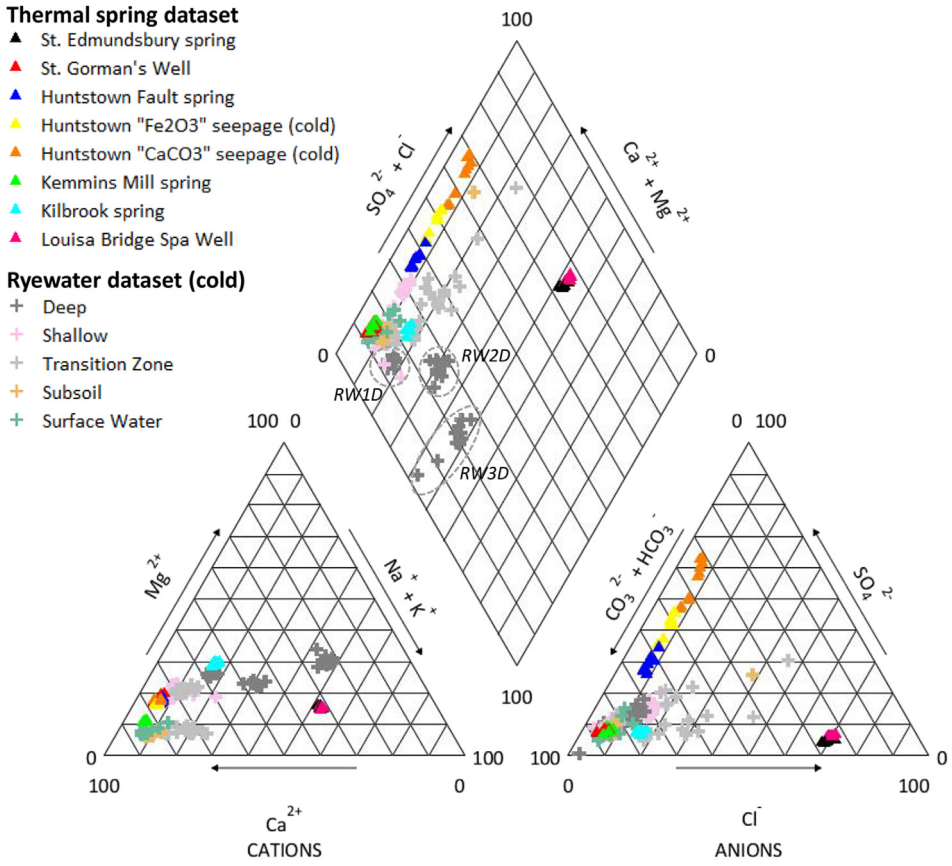

Fig. 2. Piper diagram of hydrochemical analyses from the Leinster thermal spring dataset (triangles) and cold groundwater samples from the Ryewater monitoring boreholes between June 2009 and July 2012 (crosses). Samples from the deep Ryewater boreholes form distinct clusters that are labelled. See supplementary material for a description of the installations at Ryewater.

3.2. Time-lapse temperature measurements

HOBO U24-001 loggers were installed at each of springs in July and August 2013 to record temperature and electrical conductivity (EC, μS/cm) at 15-min intervals (data from three of the thermal springs along with daily effective rainfall data for the region are presented in Fig. 3). Daily rainfall and potential evapotranspiration data from Dunsany synoptic station (Met Éireann), situated 10 km to the north of Kemmins Mill spring (Fig. 1c)), were used to calculate the effective rainfall according to the following formula (Hunter Williams et al., 2011):

$$\text{Effective rainfall} = \text{Rainfall} - 0.82(\text{Potential Evapotranspiration}). \quad (1)$$

The loggers were calibrated before installation and cross-checked against the field measurements of temperature and EC each time the data were collected. Summary statistics were calculated using the Onset HOBOWare® software (Version 3.4.1) (Table 3). For St. Gorman's Well, data are missing for the period between July 28th and August 6th, 2013 due to instrument failure. For St. Edmundsbury spring, the period between July 2013 and February 2014 shows the influence of instrument drift on the temperature readings (gradual increase in temperature during this period). The logger was repaired and redeployed in May 2014. In general, the temperature readings were more reliable than the EC readings. Due to the aerated nature of the spring waters, the EC measurements were susceptible in most cases to the influence of fouling by bacterial growths on the sensors. Those questionable EC readings that may have been affected by fouling have been indicated in Fig. 3. The quality of the EC data for St. Edmundsbury spring was particularly poor due to build-up of iron-oxide deposits on the sensor, but these data have been included here for completeness.

4. Statistical procedures

The procedure followed in this study for compositional MSA of the hydrochemical data is illustrated in Fig. 4. A standard statistical analysis was also carried out using the raw, new data for comparison with the CoDa approach (see Supplementary material).

4.1. Data preparation

Ionic balance errors for the new data were calculated using PhreeqC (version 2.18) (Parkhurst and Appelo, 1999) with the minteq.dat database. The majority of samples had calculated ionic balance errors below the recommended standard of ±5% (Freeze and Cherry, 1979), and 11 out of a total of 78 samples had elevated errors of between ±5% and ±10%. All 78 samples were retained for further analysis as the ionic balance error of 10% was deemed acceptable (Güler et al., 2002; Cloutier et al., 2008; King et al., 2014).

Only compositional hydrochemical data, i.e., ionic concentrations in mg/L or ppm, were included for the statistical analysis (temperature, pH and electrical conductivity were not included). Data expressed in ppb were converted to ppm prior to analysis. Any variables with a large proportion of samples below the LOQ (>33%

Table 2
Major, minor and trace analytes, limits of quantification and methods of analysis. For each analyte, the number of samples with levels below the LOQ is given as a percentage (total number of samples, including duplicates, is 78).

	Analyte	Measured units	LOQ	Method of analysis	% LOQ
Major ions (>1 ppm)	Ca	ppm	0.05	ICP-MS	0
	Cl	ppm	1	ICP-MS	0
	K	ppm	0.05	ICP-MS	0
	Mg	ppm	0.05	ICP-MS	0
	Na	ppm	0.05	ICP-MS	0
	Sr	ppb	0.01	ICP-MS	0
	HCO_3	ppm $CaCO_3$	10	Titralab	0
	SO_4	ppm	1	Spectrophotometry	0
	Si	ppm	1	Spectrophotometry	0
Minor & trace ions	NH_3	ppm N	0.007	Spectrophotometry	19.23
	NH_4	ppm	0.009	Spectrophotometry	19.23
	F	ppm	0.1	Ion chromatography	5.13
	As	ppb	0.5	ICP-MS	32.05
	B	ppb	5	ICP-MS	1.28
	Ba	ppb	0.05	ICP-MS	0
	Br	ppb	5	ICP-MS	0
	Co	ppb	0.02	ICP-MS	33.33
	Cs	ppb	0.01	ICP-MS	0
	Cu	ppb	0.1	ICP-MS	0
	Li	ppb	0.1	ICP-MS	0
	Mn	ppb	0.05	ICP-MS	2.56
	Mo	ppb	0.1	ICP-MS	0
	P	ppb	10	ICP-MS	1.28
	Rb	ppb	0.01	ICP-MS	0
	Rh	ppb	0.01	ICP-MS	14.1
	Sb	ppb	0.05	ICP-MS	25.64
	Se	ppb	0.5	ICP-MS	5.13
	Tl	ppb	0.01	ICP-MS	12.82
	U	ppb	0.02	ICP-MS	0
	Zn	ppb	0.5	ICP-MS	0

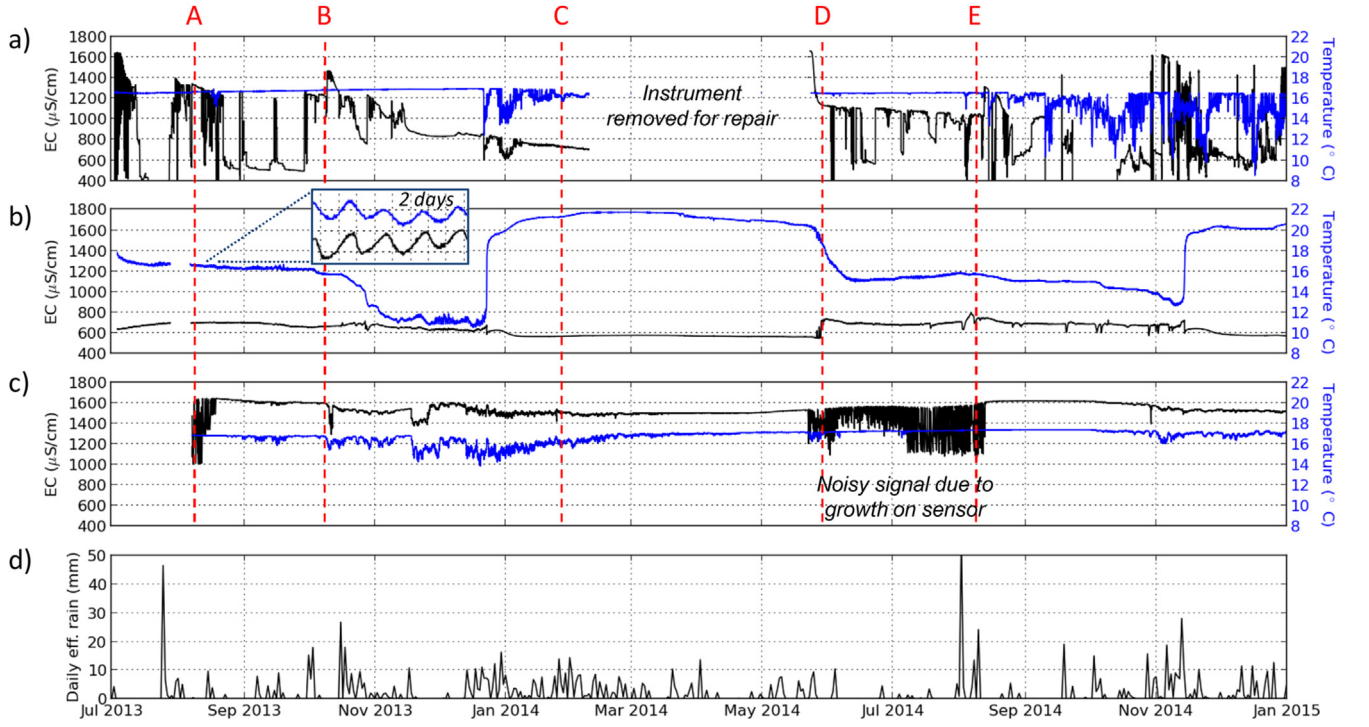

Fig. 3. Time-lapse temperature (blue) and electrical conductivity (black) measurements. a) St. Edmundsbury spring. b) St. Gorman's Well (inset shows semi-diurnal fluctuations over two days in August 2013). c) Louisa Bridge Spa Well. d) Daily effective rainfall data calculated from Met Éireann data (Dunsany synoptic station, Meath). Hydrochemical sampling seasons are indicated in red (A = July/August 2013, B = October 2013, C = January 2014, D = May 2014, E = August 2014). Data is missing for St. Edmundsbury spring between February and May 2014 due to failure of the data logger; likewise for St. Gorman's Well in August 2013. Evidence of fouling (growth on sensor) as a result of incorrect positioning of the logger is indicated for Louisa Bridge Spa Well.

Table 3
Summary statistics for non-compositional data from the thermal springs. Temperature (T) and electrical conductivity (EC) data from time-lapse logger measurements. Generally, electrical conductivity data were far less reliable than temperature data due to frequent fouling of the sensors. pH measured in field with Hanna Combo meter during hydrochemical sampling rounds.

Spring	pH range	Max EC (μS/cm)	Max T (°C)	Min T (°C)	Mean T (°C)	σ T
St. Edmundsbury spring	7.37–7.67	1664	17.0	8.5[a]	16.2[a]	1.01[a]
St. Gorman's Well	6.7–7.8	790	21.8	10.5	17.2	3.1
Huntstown Fault spring	6.68–7.7	1049	16.3	15.0	15.5	0.35
Kemmins Mill spring	6.9–7.56	520	14.9	14.1	14.3	0.2
Kilbrook spring	6.71–7.8	723	25.0	19.5	23.9	0.65
Louisa Bridge Spa Well	6.95–7.77	1644	17.5	13.9	16.8	0.57

[a] St. Edmundsbury temperature minimum due to flooding – not representative of thermal groundwater.

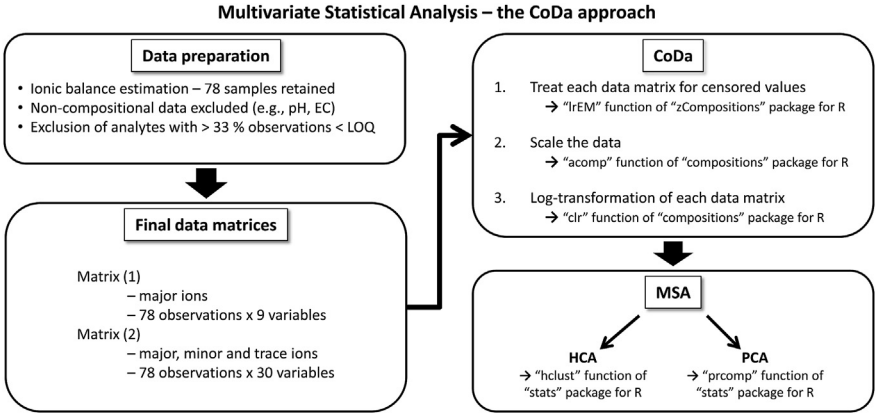

Fig. 4. Methodological flow-chart illustrating steps taken in compositional data analysis and MSA.

of samples below the LOQ) were discarded. The discarded variables included NO_3, Fe, Ni, Cr and Pb. The data matrix for the thermal springs and cold seepages (including trace element data – called Matrix (2)) consisted of 78 observations and 30 variables (Table 2).

As defined by Krešić (2007), a major constituent element of groundwater is one with a concentration greater than 1 mg/L. On this basis, a subset of nine major ions (Ca, K, Mg, Na, Cl, HCO_3, SO_4, Si and Sr) was chosen from the thermal dataset. A new matrix using these major ions was compiled (Matrix (1)) containing 78 observations and 9 variables.

4.2. Compositional data analysis (CoDa)

It is critically important that the compositional nature of environmental data be taken into consideration for practically any aspect of statistical data analysis (Filzmoser et al., 2009a), as a failure to do so has been shown to generate misleading results (e.g., Otero et al., 2005; Wang et al., 2014; see also the Supplementary material). Compositional data can be treated prior to statistical analysis by using a family of log-ratio transforms (Aitchison, 1986; Egozcue et al., 2003) to convert the original compositional data into new coordinates, which follow the rules of Euclidean geometry in real space. CoDa tools for the processing and transformation of compositional data are freely available through the R statistical environment (version 3.10.1) (R Development Core Team, 2015). Some of these tools have been used in this work (Fig. 4), in particular the packages "compositions" (Van den Boogaart and Tolosana-Delgado, 2008) and "zCompositions" (Palarea-Albaladejo and Martín-Fernández, 2015).

A variation matrix (Aitchison, 1986) was generated to examine the data (Table 4). Each component of the variation matrix, τ, describes the log-relationship between two variables x_i and x_j (in this case chemical analytes), and is defined as

$$\tau_{ij} = \mathrm{var}\left(\ln \frac{x_i}{x_j}\right), \tag{2}$$

and estimated by

$$\tau_{ij} = \frac{1}{N-1}\sum_{n=1}^{N} \ln^2 \frac{x_{ni}}{x_{nj}} - \ln^2 \frac{\overline{g}_i}{\overline{g}_j}, \tag{3}$$

where N is the number of observations and $\overline{g}_i$, $\overline{g}_j$ are the geometric mean values for the two variables in question. A small value of τ_{ij} (which is equivalent to τ_{ji}) implies a good proportionality between two variables. An index of proportionality (first introduced by Aitchison as an "approximate correlation coefficient"), ρ, for any pair of variables, i and j, can be estimated using the following transformation:

$$\rho_{ij} = \exp\left(-\frac{\tau_{ij}^2}{2}\right), \tag{4}$$

(Van den Boogaart and Tolosana-Delgado, 2013) (Table 4). Strong relationships between pairs of variables have an index close to 1. The indices reveal a perfectly proportional relationship between NH_3 and NH_4 ($\rho = 1$) which is sensible as the NH_4 values were calculated from the measured ammonia values by the analytical laboratory (NH_3 measured as N in mg/L). Proportional relationships ($\rho > 0.99$) also exist for the major ion pairs [Na, Cl] and [Ca, HCO_3].

Since CoDa techniques treat all components of the composition simultaneously, the absence of data or the presence of censored values in a compositional dataset can prevent the application of the log-transformation approach (Palarea-Albaladejo et al., 2014; Buccianti et al., 2014). In this work, the log-ratio Expectation-

Table 4
Variation matrix for thermal spring hydrochemistry dataset (30 variables). The lower triangle provides the variation element (τij) for all variable pairs – the smaller the variation element, the greater the proportionality between the two variables. The upper triangle contains a transformation of each variation element, which provides an approximate index of proportionality for each variable pair. Those proportionality indices indicating very strong relationships (>0.8) are highlighted in bold text.

	As	B	Ba	Br	Ca	Cl	Co	Cs	Cu	K	Li	Mg	Mn	Mo	Na	P	Rb	Rh	Sb	Se	Sr	Tl	U	Zn	HCO_3	SO_4	Si	F	NH_3	NH_4
As		0.07	0.46	0.24	0.01	0.33	0.04	0.19	0.00	0.16	0.21	0.10	0.00	0.10	0.34	0.00	0.30	0.17	0.00	0.00	0.22	0.00	0.00	0.00	0.01	0.01	0.01	0.09	0.02	0.01
B	2.30		**0.91**	**0.93**	**0.97**	0.50	0.02	0.15	0.69	**0.95**	0.16	**0.99**	0.00	**0.87**	0.65	**0.94**	**0.82**	**0.96**	0.64	**0.89**	**0.98**	0.32	**0.80**	0.33	**0.96**	0.74	0.75	**0.99**	0.11	0.11
Ba	1.25	0.42		**0.85**	0.70	0.59	0.11	0.15	0.62	**0.84**	0.26	**0.91**	0.00	0.69	0.71	0.52	0.78	**0.90**	0.43	0.45	**0.94**	0.19	0.35	0.16	0.60	0.69	0.50	**0.90**	0.05	0.05
Br	1.69	0.39	0.57		0.78	**0.94**	0.01	0.61	0.33	**1.00**	0.63	**0.95**	0.00	0.66	**0.97**	0.76	**0.99**	**0.98**	0.28	0.79	**0.99**	0.10	0.27	0.26	0.79	0.30	0.71	**0.94**	0.21	0.21
Ca	3.16	0.25	0.85	0.70		0.16	0.01	0.02	**0.90**	**0.87**	0.01	**0.98**	0.00	0.76	0.28	**0.97**	0.54	**0.86**	0.72	**0.94**	**0.89**	0.29	**0.97**	0.56	**1.00**	**0.85**	**0.91**	**0.98**	0.06	0.06
Cl	1.49	1.17	1.02	0.34	1.90		0.00	**0.90**	0.01	**0.90**	**0.95**	0.55	0.00	0.23	**1.00**	0.18	**0.98**	**0.80**	0.02	0.26	**0.85**	0.00	0.01	0.02	0.18	0.02	0.16	0.51	0.06	0.06
Co	2.50	2.75	2.09	3.09	3.20	3.88		0.00	0.01	0.01	0.00	0.03	0.08	0.06	0.00	0.01	0.00	0.03	0.00	0.00	0.03	0.04	0.00	0.00	0.02	0.00	0.01	0.02	0.00	0.00
Cs	1.81	1.94	1.94	0.99	2.84	0.45	4.26		0.00	0.55	**0.99**	0.25	0.00	0.19	**0.91**	0.07	**0.87**	0.45	0.00	0.07	0.52	0.00	0.00	0.00	0.05	0.00	0.04	0.20	0.00	0.00
Cu	3.47	0.87	0.98	1.49	0.45	2.99	3.10	4.27		0.40	0.00	0.74	0.00	0.43	0.03	0.64	0.13	0.46	0.71	0.53	0.51	0.27	**0.86**	0.50	0.79	**0.90**	0.73	0.76	0.01	0.01
K	1.91	0.30	0.58	0.05	0.53	0.47	3.25	1.09	1.34		0.54	**0.98**	0.00	0.73	**0.95**	**0.83**	**0.99**	**0.99**	0.44	**0.88**	**1.00**	0.14	0.40	0.35	**0.87**	0.39	0.74	**0.97**	0.16	0.15
Li	1.76	1.91	1.65	0.96	2.91	0.33	4.08	0.17	4.14	1.10		0.25	0.00	0.13	**0.95**	0.04	**0.87**	0.46	0.00	0.07	0.56	0.00	0.00	0.00	0.03	0.00	0.03	0.20	0.00	0.00
Mg	2.13	0.13	0.43	0.32	0.22	1.09	2.65	1.67	0.78	0.22	1.66		0.00	**0.93**	0.71	**0.96**	**0.89**	**0.98**	0.70	**0.94**	**0.99**	0.42	**0.82**	0.37	**0.98**	0.69	**0.90**	**1.00**	0.07	0.07
Mn	5.38	6.30	5.67	6.36	6.93	6.85	2.25	7.56	7.39	6.58	7.38	6.44		0.00	0.00	0.00	0.00	0.00	0.00	0.00	0.00	0.00	0.00	0.00	0.00	0.00	0.00	0.00	0.00	0.00
Mo	2.14	0.52	0.86	0.92	0.75	1.71	2.37	1.81	1.30	0.79	2.01	0.38	5.74		0.38	**0.86**	0.67	0.79	0.34	0.57	**0.85**	0.24	0.64	0.08	**0.85**	0.33	0.74	**0.91**	0.02	0.02
Na	1.46	0.93	0.83	0.24	1.59	0.02	3.59	0.43	2.63	0.33	0.33	0.83	6.72	1.39		0.31	**0.99**	**0.89**	0.05	0.40	**0.93**	0.02	0.02	0.04	0.31	0.04	0.26	0.67	0.06	0.06
P	3.37	0.34	1.15	0.74	0.24	1.85	2.97	2.33	0.94	0.61	2.49	0.28	6.79	0.56	1.53		0.58	**0.84**	0.44	**0.93**	**0.89**	0.49	**0.90**	0.47	**1.00**	0.41	**0.92**	**0.94**	0.03	0.03
Rb	1.54	0.62	0.71	0.14	1.12	0.20	3.35	0.52	2.04	0.13	0.52	0.49	6.65	0.90	0.11	1.04		**0.95**	0.20	0.65	**0.98**	0.07	0.11	0.12	0.59	0.12	0.49	**0.87**	0.08	0.08
Rh	1.88	0.28	0.46	0.20	0.55	0.66	2.67	1.26	1.24	0.17	1.24	0.22	6.05	0.69	0.49	0.58	0.32		0.37	**0.82**	**0.99**	0.24	0.47	0.30	**0.87**	0.43	0.73	**0.96**	0.09	0.09
Sb	3.68	0.94	1.29	1.60	0.80	2.84	4.68	3.83	0.82	1.29	3.69	0.85	9.55	1.46	2.48	1.27	1.80	1.40		0.70	0.44	0.09	0.73	0.06	0.54	**0.82**	0.34	0.70	0.00	0.00
Se	3.74	0.48	1.26	0.69	0.35	1.64	4.30	2.29	1.13	0.50	2.29	0.34	8.71	1.05	1.36	0.37	0.92	0.62	0.84		**0.87**	0.31	0.77	0.34	**0.94**	0.43	0.79	**0.93**	0.01	0.01
Sr	1.74	0.20	0.35	0.11	0.48	0.56	2.59	1.14	1.16	0.08	1.08	0.10	6.12	0.57	0.39	0.48	0.21	0.11	1.28	0.52		0.30	0.51	0.34	**0.91**	0.46	**0.81**	**0.99**	0.11	0.11
Tl	4.67	1.51	1.83	2.14	1.57	3.27	2.51	3.64	1.62	1.98	3.35	1.31	7.20	1.69	2.85	1.19	2.29	1.70	2.17	1.53	1.55		0.30	0.39	0.48	0.03	0.25	0.33	0.00	0.00
U	4.15	0.66	1.46	1.61	0.26	3.25	3.36	4.12	0.55	1.35	4.22	0.62	7.46	0.94	2.82	0.47	2.10	1.24	0.79	0.71	1.16	1.54		0.23	**0.94**	0.79	0.71	**0.82**	0.01	0.01
Zn	4.66	1.49	1.90	1.63	1.08	2.80	3.51	3.94	1.18	1.46	3.85	1.41	7.07	2.22	2.54	1.24	2.06	1.56	2.39	1.47	1.47	1.37	1.72		0.62	0.09	0.45	0.37	0.00	0.00
HCO_3	3.21	0.30	1.01	0.68	0.10	1.84	2.84	2.49	0.68	0.53	2.61	0.21	6.46	0.56	1.53	0.09	1.03	0.53	1.11	0.35	0.44	1.22	0.34	0.98		0.57	**0.94**	**0.97**	0.05	0.05
SO_4	3.14	0.78	0.86	1.56	0.58	2.86	3.86	4.34	0.46	1.37	4.19	0.86	7.91	1.49	2.53	1.34	2.06	1.30	0.63	1.30	1.24	2.69	0.69	2.21	1.07		0.38	0.73	0.02	0.02
Si	3.16	0.76	1.18	0.83	0.43	1.93	3.10	2.55	0.79	0.78	2.63	0.46	7.05	0.77	1.64	0.42	1.19	0.80	1.47	0.68	0.65	1.66	0.82	1.26	0.34	1.39		**0.89**	0.04	0.04
F	2.20	0.15	0.46	0.36	0.21	1.16	2.90	1.79	0.74	0.25	1.79	0.04	6.67	0.43	0.89	0.34	0.54	0.27	0.84	0.38	0.16	1.49	0.63	1.41	0.23	0.80	0.49		0.07	0.07
NH_3	2.90	2.10	2.42	1.76	2.34	2.36	4.62	3.55	3.18	1.93	3.64	2.32	6.52	2.73	2.36	2.64	2.23	2.20	3.45	2.99	2.08	5.35	3.22	3.79	2.46	2.88	2.53	2.32		**1.00**
NH_4	2.90	2.10	2.42	1.77	2.35	2.36	4.63	3.55	3.18	1.93	3.64	2.33	6.52	2.73	2.36	2.64	2.23	2.20	3.45	3.00	2.09	5.36	3.23	3.80	2.46	2.88	2.53	2.32	0.00	

Maximisation algorithm of Palarea-Albaladejo and Martín-Fernández (2008) was used to replace the censored values. This procedure uses the information in the covariance structure to produce a conditional estimate of the censored values whilst preserving the ratios between those observations without censored values (Palarea-Albaladejo et al., 2014).

In this study, the centred-log-ratio (clr) transformation was applied to each of the raw data matrices. The clr-transformation uses the geometric mean of the data as a denominator to represent compositional data as a real vector. For a matrix, **x**, of *D* parts:

$$\mathrm{clr}(\mathbf{x}) = \left(\ln \frac{x_i}{g(\mathbf{x})}\right)_{i=1,\ldots,D}, \text{ where } g(\mathbf{x}) = \sqrt[D]{x_1 \cdot x_2 \cdot \ldots \cdot x_D}. \quad (5)$$

This transformation was developed by Aitchison (1986) and is commonly used for covariance-based PCA (Drew et al., 2008; Engle and Blondes, 2014; see also Filzmoser et al., 2009b). In this analysis, no closure operation was applied to the data (see Palarea-Albaladejo and Martín-Fernández, 2015).

4.3. Multivariate statistical analysis (MSA)

MSA tools, such as HCA and PCA, are proven techniques for the exploration of large hydrochemical datasets (recent CoDa-compatible examples include Buccianti and Grunsky (2014), and Engle and Rowan (2014)). In this work, MSA was applied to decipher the underlying processes affecting the hydrochemistry of the thermal springs. It is important to note that while MSA allows for samples to be grouped by similar physical and chemical properties, it does not immediately identify which trends or processes may be important in controlling the composition of the groundwater (Güler et al., 2002). It is therefore important to consider the results of MSA in conjunction with other available data to interpret the underlying structure in the dataset in a meaningful way.

4.3.1. Hierarchical cluster analysis (HCA)

Cluster analysis is a family of multivariate techniques designed to uncover and classify naturally occurring subgroups within a dataset based upon similarities between the observations. HCA seeks to build a hierarchy of clusters, and can also be applied to compositional data that are log-transformed (Van den Boogaart and Tolosana-Delgado, 2013). Agglomerative HCA (Euclidean distance (equivalent to the Aitchison distance (Aitchison et al., 2000)) and Ward's linkage method were used) was applied to the clr-transformed data of Matrix (2) to group the water samples based upon similarities in their hydrochemistry. Visual examination of the dendrogram suggests the presence of six strongly distinct clusters (Fig. 5).

4.3.2. Principal component analysis (PCA)

PCA is a technique that attempts to elucidate an underlying structure to a dataset (Davis, 1986), and is particularly useful for exploring large datasets as it effectively reduces the number of parts (or variables) in the dataset. It is a well-proven technique for hydrochemical scenarios, including the investigation of thermal spring water provenance (Helena et al., 2000; Tanasković et al., 2012), although the usual approach, as exemplified by the examples cited, is to use a classical PCA on raw hydrochemical data. Here, the PCA was performed on appropriately log-transformed data following the CoDa approaches of Otero et al. (2005), Engle and Rowan (2014) and Engle et al. (2014). The PCA operation extracts the principal components, or loadings, by singular value decomposition (SVD) of the (clr-transformed) data matrix. The SVD produces a new matrix of standardized coordinates for each sample, called the scores, and a new matrix of variable loadings with columns representing the principal components.

Graphical representations of the PCA results were interpreted using biplot analysis (Gabriel, 1971), in which the samples are represented as points and the variables as arrows, or rays. The interpretation of the covariance biplot has been adapted for compositional data (Aitchison and Greenacre, 2002). Once the compositional data has been transformed, meaningful statements may only be made involving ratios of components (Buccianti and Grunsky, 2014). In a compositional covariance biplot, the rays of the biplot cannot be directly interpreted as each has a complex relationship to all of the original variables, so the links between ray vertices are more important for interpretation. The length of a ray generally represents the communality of the variable, or how much of the total variance is represented by that variable (Otero et al., 2005). The higher the proportion of the total variance represented by the biplot, the better and more trustworthy the representation of the variables involved. For compositional covariance biplots, the following rules of interpretation apply (subject to the proportion of total variance explained by the biplot): 1) if two

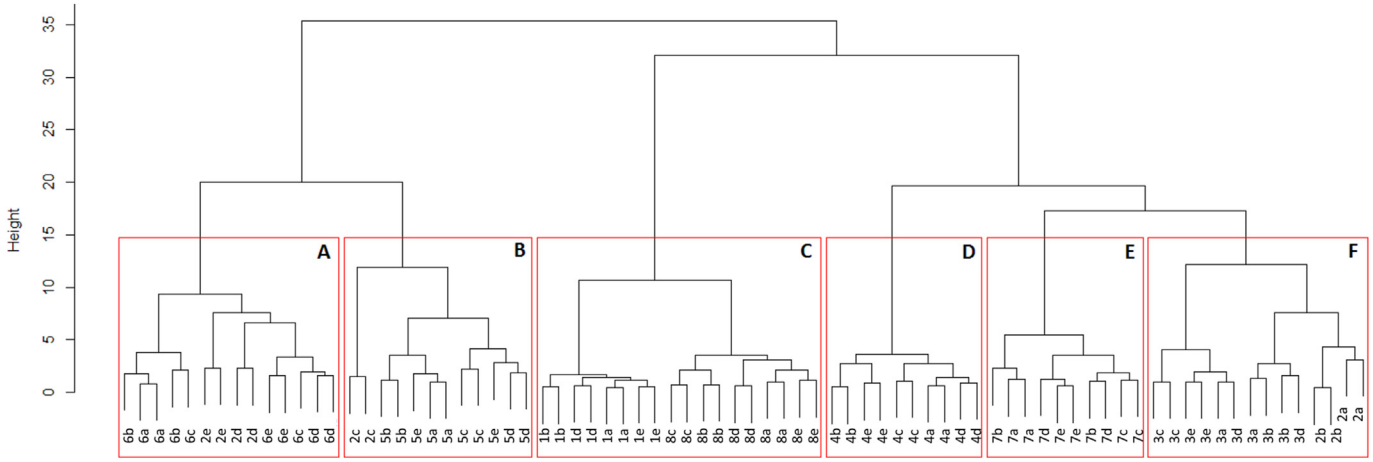

Fig. 5. Cluster analysis dendrogram for compositional agglomerative HCA of Matrix (2). The HCA has clustered the samples into six distinct groups according to their chemical similarities, labelled A to F. Samples are numbered according to spring: 1) St. Edmundsbury spring; 2) St. Gorman's Well; 3) Huntstown Fault spring; 4) Huntstown Fe_2O_3 cold seepage; 5) Huntstown $CaCO_3$ cold seepage; 6) Kemmins Mill spring; 7) Kilbrook spring; and 8) Louisa Bridge Spa Well. They are also labelled according to the season in which the sample was collected: A. August 2013; B. October 2013; C. January 2014; D. May 2014; and E. August 2014. Duplicate samples for each spring were collected.

vertices are coincident or situated close to each other, they are proportional; 2) the length of a link between two vertices is proportional to the log ratio of those two variables; 3) if three or more vertices lie on the same link, they may represent a sub-composition with one single degree of freedom; and 4) if two links between four separate clr-variables are orthogonal then the corresponding pairs of variables may vary independently of each other (this also applies for two orthogonal links describing sub-compositions).

5. Compositional MSA results

5.1. HCA

The HCA of the thermal spring data (Matrix (2)) identified six main clusters of samples (Fig. 5). These clusters mostly correspond to individual springs, but with some exceptions. St. Edmundsbury spring and Louisa Bridge Spa Well are grouped into one cluster (C), indicating a very close similarity between the two. The remaining five clusters, A, B, D, E and F contain samples from Kemmins Mill spring, Huntstown "$CaCO_3$" cold seepage, Huntstown "Fe_2O_3" cold seepage, Kilbrook spring and Huntstown Fault spring respectively. Samples from St. Gorman's Well are distributed between three clusters (A, B and F). The samples collected from St. Gorman's Well in July/August and October 2013 are most similar to the warm spring from Huntstown Fault (F); samples collected in January 2014 are grouped with Huntstown "$CaCO_3$" cold seepage (B); and the samples from May and August 2014 are grouped with the warm spring at Kemmins Mill (A). The HCA suggests that St. Gorman's Well had the largest variation in hydrochemistry throughout the sampling period; this is corroborated by the time-lapse temperature and electrical conductivity measurements (Table 3 and Fig. 3), which show that St. Gorman's Well also has the largest variation in temperature throughout the year.

5.2. PCA

PCA was applied separately to Matrix (1) and Matrix (2). The number of observations for the thermal spring data included duplicate measurements, and these are indicated clearly in Fig. 6. The inclusion of these duplicates in the PCA does not appreciably affect the outcomes or interpretation, but illustrates the reliability and quality of the measurements. PCA of Matrix (1) investigated the hydrogeological processes controlling the major ion concentrations and overall hydrochemistry within the group of thermal springs, and PCA of Matrix (2) investigated the more subtle effects of any hydrogeological processes impacting the trace element hydrochemistry of the thermal waters.

5.2.1. Matrix (1): major ions (9 variables)

The scree plot of variance in Fig. 7a) "breaks" after the second component (i.e., there is a sudden and marked change in slope), indicating that a biplot of the first two PCs will provide a trustworthy representation of the data (they represent 91.1% of the total log-ratio (clr) variance in the dataset). The compositional covariance biplot (Fig. 6a)) shows the highest clr-variances for SO_4 and Si, followed by Cl and Na, and the lowest clr-variances for K, Sr and Mg. The PCA has grouped the samples from Louisa Bridge Spa Well, St. Edmundsbury spring and Kilbrook spring separately in the western quadrants of the biplot. Samples from the remaining springs and cold seepages are located in the eastern quadrants of the biplot and appear to be more disperse. There is overlap between samples from St. Gorman's Well and Kemmins Mill spring in the northeast quadrant and the three sampling points from Huntstown plot near to each other in the southeast quadrant. Samples from St. Gorman's Well have the largest dispersion in the biplot, indicating that it has the highest clr-variance. On the basis of this plot, which explores the major ion chemistry only, St. Gorman's Well does not follow the temporal variation pattern revealed by the HCA, but appears to behave similarly to Kemmins Mill spring for all sampling seasons.

The main inferences arising from the biplot in Fig. 6a) are:

- The vertices for Na and Cl lie close to each other; this indicates their proportionality (verified by the very low clr-variance of [Na, Cl]; 0.35% of total clr-variance). The samples from Louisa Bridge Spa Well and St. Edmundsbury spring are strongly associated with Na and Cl.
- It is possible to draw a link between the vertices of Cl, Na, K, and Sr, indicating that these variables may form a sub-composition with a single degree of freedom.
- The vertices of SO_4, Ca, HCO_3 and Si lie on a common link, forming a sub-composition with one degree of freedom. This link is almost orthogonal to the link drawn between Cl, Na, K, and Sr, suggesting that these two sub-compositions may vary independently of each other. Ca could lie on either link, however, the sub-compositions are more orthogonal to each other, and therefore more independent of each other, when the variables are distributed between them as [Cl, Na, K, Sr] and [SO_4, Ca, HCO_3, Si] (this was checked by calculating the correlation between the first singular vectors for each sub-composition – see Van den Boogaart and Tolosana-Delgado, 2013).
- The two links can be interpreted as two independent influencing processes, or sets of processes, on the hydrochemistry of the springs: the "water-rock interaction" link ***S*** [Cl, Na, K, Sr] representing the increased association with saline, Na-Cl-type waters towards the Na/Cl end of the link, and perhaps increased residence times towards the K/Sr end of the link; and the "carbonate" link ***C*** [SO_4, Ca, HCO_3, Si] representing the dissolution of different types of carbonate bedrock (HCO_3 at one end of the link and SO_4 at the other end).
- St. Edmundsbury spring and Louisa Bridge Spa Well have a strong association with the Na/Cl end of link ***S***. Samples in the eastern quadrants of the biplot are more disperse and have a stronger association with the ***C*** link; they range from having an association with the SO_4 end of the link (the Huntstown sampling locations) to being more strongly associated with HCO_3 and Si (St. Gorman's Well and Kemmins Mill).

5.2.2. Matrix (2): major, minor and trace ions (30 variables)

There is a "break" in slope of the scree plot after the fourth PC (Fig. 7b)) with these four PCs accounting for 85.6% of the total clr-variance of the dataset. Biplot analysis of the first two PCs accounts for just 61% of the total variance. The total variance of the dataset is dominated by Mn which has the highest communality, followed by Co (23.09 and 10.47% of the total clr-variance respectively). These two variables lie in the northwest quadrant. The sub-composition [Li, Cs, Na, Cl] is situated in the southwest quadrant and represents just 1.52% of the total clr-variance, indicating a proportional relationship between those elements. The sub-composition [SO_4, Ca, HCO_3, Si] is situated in the northeast quadrant and represents 3.39% of the total clr-variance, indicating a proportional relationship. The clusters from Fig. 5 are once again clearly defined in terms of the distribution of the samples in Fig. 6b). Compared to Fig. 6a), the samples from St. Edmundsbury spring and Louisa Bridge Spa Well lie further away from each other in the southwest quadrant, indicating subtle differences in hydrochemistry, which are evident upon comparison of their trace element chemistries. The samples from Huntstown are also more disperse: samples from Huntstown "Fe_2O_3" cold seepage and the Huntstown Fault spring lie mainly in the northwest quadrant

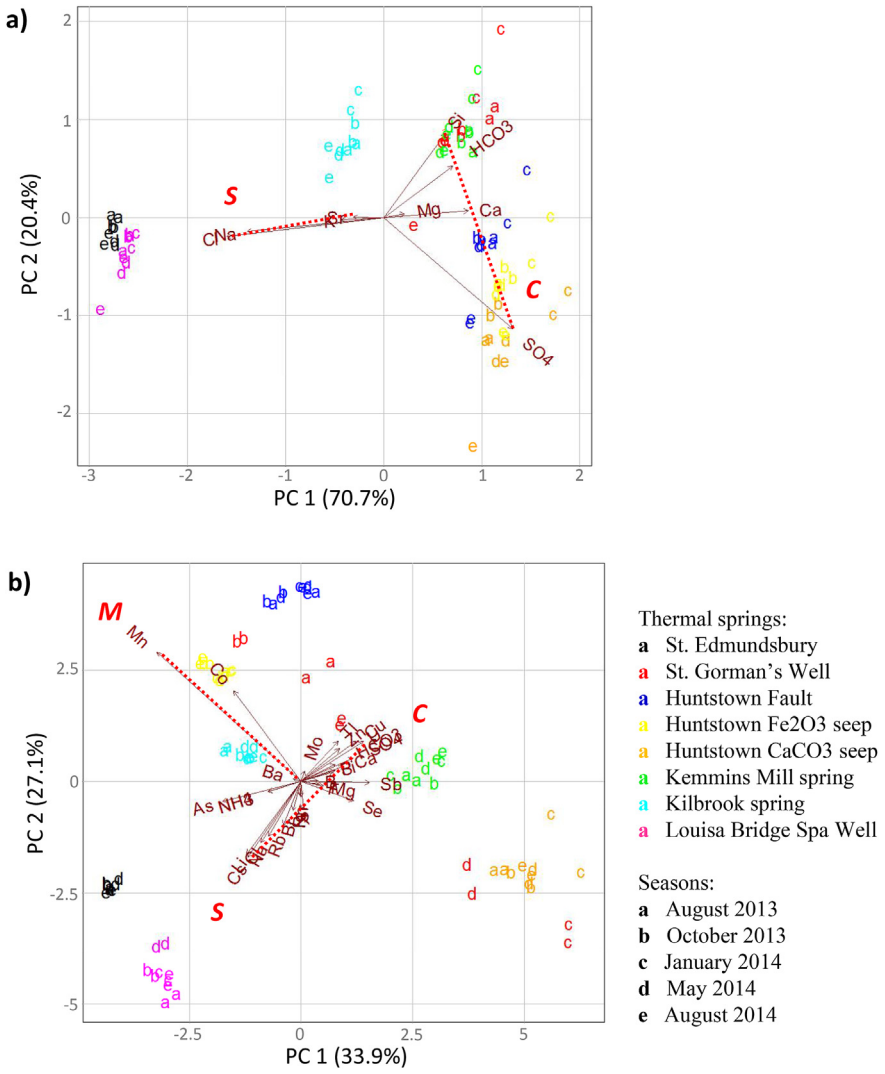

Fig. 6. Compositional PCA biplots: a) Matrix (1) (see section 4.1), orthogonal links ***S*** and ***C*** are indicated; b) Matrix (2), orthogonal links ***M***, and ***S*** − ***C*** are indicated. Hydrochemical sampling seasons are indicated as follows: a = Jul/Aug 2013, b = Oct 2013, c = Jan 2014, d = May 2014, e = Aug 2014. Duplicate samples for each spring were collected.

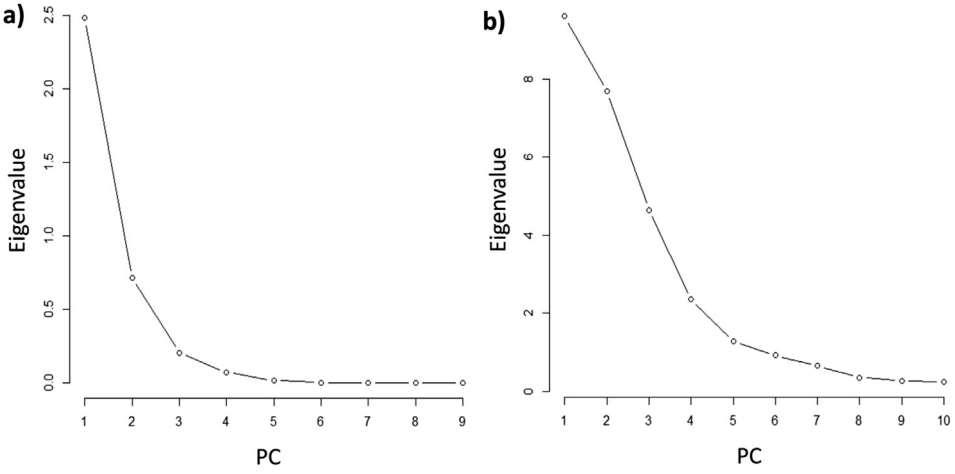

Fig. 7. Scree plots of the variance represented by each principal component for each data matrix: a) Matrix (1); and b) Matrix (2).

whereas samples from Huntstown "$CaCO_3$" cold seepage lie in the opposite corner of the biplot. Samples from St. Gorman's Well show a remarkably large, almost linear dispersion in the biplot, from northwest to southeast.

The main inferences that may be discerned from the biplot in Fig. 6b) are:

- There appears to be a common link between the following variables from southwest to northeast on the biplot: Li, Cs, Cl, Na, Rb, Br, K, Sr, Mg, Si, HCO_3, Ca, and SO_4. The link between them represents a continuum between the two independent hydrogeological processes identified in Fig. 6a), and processes ***S*** [Na, Cl, K, Sr] and ***C*** [Si, HCO_3, Ca, SO_4] form endmembers of an axis (the link ***S*** − ***C***) representing the trade-off between saline and calcium-bicarbonate groundwaters in the dataset.
- As expected, St, Edmundsbury spring and Louisa Bridge Spa Well have the greatest association with the ***S*** end of the link ***S*** − ***C***, and their hydrochemistry is clearly governed by increased salinity. Moving along the ***S*** − ***C*** link, Kemmins Mill spring, St. Gorman's Well and the samples from Huntstown are shown to have an association with the ***C*** end of the link.
- The link between Mn and Ba is orthogonal to the link ***S*** − ***C***; this orthogonality was checked by calculating the correlation between the first singular vectors for each sub-composition (Van den Boogaart and Tolosana-Delgado, 2013), which was found to be very low (a value of 0.07), thus the links are independent. This new link is called ***M*** and is independent of processes ***S*** and ***C***. Link ***M*** represents the processes of mineralisation and the dissolution of mineral sulfides, sulfates and oxides hosted in the carbonate bedrock, particularly those containing Mn at one end of the link, and Ba at the other. Barite and manganese are sometimes associated with the massive sulfide deposits found in Irish Lower Carboniferous limestones (e.g., Cole, 1922; Boyce et al., 2003).
- Samples in the northwest quadrant of the biplot have a stronger association with the Mn end of link ***M***, such as samples from Huntstown "Fe_2O_3" cold seepage and Huntstown Fault spring, which also have the highest Fe content.
- Data from St. Gorman's Well is widely dispersed in the biplot. At all times, the data from St. Gorman's Well has a stronger association with the ***C*** end of the ***S*** − ***C*** link. The greatest seasonal variation in chemistry occurs along the axis of link ***M***. The spring has the closest association with the Mn end of link ***M*** in the low-recharge period (seasons "a" and "b").

6. Discussion

The CoDa approach to MSA provides a deeper insight into the hidden structure of the thermal spring data than a standard statistical approach. The results of the two PCAs were used to identify three links ("***S***", "***C***", and "***M***"), which represent important underlying processes that are likely to control the hydrochemistry of the thermal springs. The two most important processes that govern the major ion hydrochemistry, ***S*** and ***C***, are independent and define the major ion hydrochemistry (Fig. 6a). When more parts (minor and trace ions) are added to the thermal dataset, the picture becomes less clear with less of the total variance represented by the biplot (Fig. 6b); this is due to the fact that for compositional data, trace element concentrations typically exhibit large log-ratio variances but low Euclidean variances (the concentrations are small by definition) (see: Otero et al., 2005; Engle et al., 2014). In Fig. 6b) processes ***S*** and ***C*** form endmembers of an axis (the link ***S*** − ***C***), which is orthogonal to link ***M***, indicating that process ***M*** is independent of processes ***S*** and ***C***. Here, we discuss each of the processes in detail, and discuss how the compositional MSA has added to the understanding of the temporal variation of St. Edmundsbury spring, St. Gorman's Well and Louisa Bridge Spa Well.

6.1. S, the "water-rock interaction" link

S joins the major ions [Na, Cl, K, Sr] in Fig. 6a), and the springs with a more saline hydrochemistry (St. Edmundsbury spring and Louisa Bridge Spa Well) are associated with the Na/Cl end of the link. In Fig. 6b), the minor and trace ions Li, Cs, Rb and Br have short links to Na and Cl, and are closely associated with the ***S*** end of the ***S*** − ***C*** axis. Fluid-mobile trace elements, such as Li, Rb and Cs, are generally considered as residence-time indicators as they are progressively released from carbonate, silicate or oxide minerals in the aquifer, even during periods of low-flow (Aquilina et al., 1997; Edmunds and Smedley, 2000; Reyes and Trompetter, 2012). St. Edmundsbury spring and Louisa Bridge Spa Well have the highest electrical conductivities of the thermal springs (maxima of 1664 μS/cm and 1644 μS/cm respectively) and form their own cluster in the HCA (Fig. 5). Their representation in Fig. 2 indicates how different they are from the other thermal waters. Their strong association with the Na/Cl end of link ***S***, and with the trace elements Li, Rb and Cs, suggests they are the most influenced by salinity, and may have longer residence times. This is supported by other available data, such as legacy isotopic and inert gas measurements (Burdon, 1983) that suggest a groundwater residence time in excess of 30,000 years for Louisa Bridge Spa Well.

Kilbrook spring is most closely associated with the K/Sr end of link ***S*** indicating that K/Sr are relatively enriched in this spring compared to Na/Cl. K in groundwater is controlled by the amount and duration of progressive water-rock interactions (Edmunds et al., 2003). K comes principally from the weathering of feldspars and clay minerals, and is not typically abundant in pure carbonate bedrock. This may indicate an extra source of K to the groundwater, such as a non-carbonate lithology situated deeper in the basinal sequence, or in the basement beneath it. The most likely potential contributors of extra K to the thermal springs are the terrestrial Devonian sandstones, mudstones and conglomerates beneath the Dublin Basin. These sediments are commonly arkosic and contain detrital clastic materials from erosion and un-roofing of the Caledonian granites. The link ***S*** therefore represents the influence of salinity and increased water-rock interaction times (and increased residence times) on the groundwater chemistry, and possibly the influence of non-carbonate lithologies from basement rocks.

The relationship between Na, Cl and Br is used to provide information about the provenance and evolution of saline waters (e.g., Davis et al., 1998), and can help to determine the source of extra chloride in the groundwater. The extra chloride may be from either natural dissolution of chloride evaporites, such as halite (NaCl) or sylvite (KCl), or anthropogenic contamination (e.g., the addition of fertilizers to land, de-icing of roads or industrial practices) (Davis et al., 2001). A CoDa-compatible approach using the isometric log-ratio (ilr) transformation developed by Egozcue et al. (2003) can be used to investigate the source of the extra chloride. This method was applied in Engle and Rowan (2013) and is discussed in detail therein. The method uses the ilr-transformation to convert the compositional data (expressed here as molar concentrations for comparison) to a new coordinate system, where each point is represented by (z_2, z_1).

$$z_1 = \frac{1}{\sqrt{2}} \ln \frac{[Na]}{[Cl]}; \tag{6}$$

$$z_2 = \frac{\sqrt{2}}{\sqrt{3}} \ln \frac{\sqrt{[Na][Cl]}}{[Br]}. \tag{7}$$

In the first coordinate, z_1, Br is excluded so this provides insight into the relative gain/loss of Na compared to Cl. In z_2, Br is included

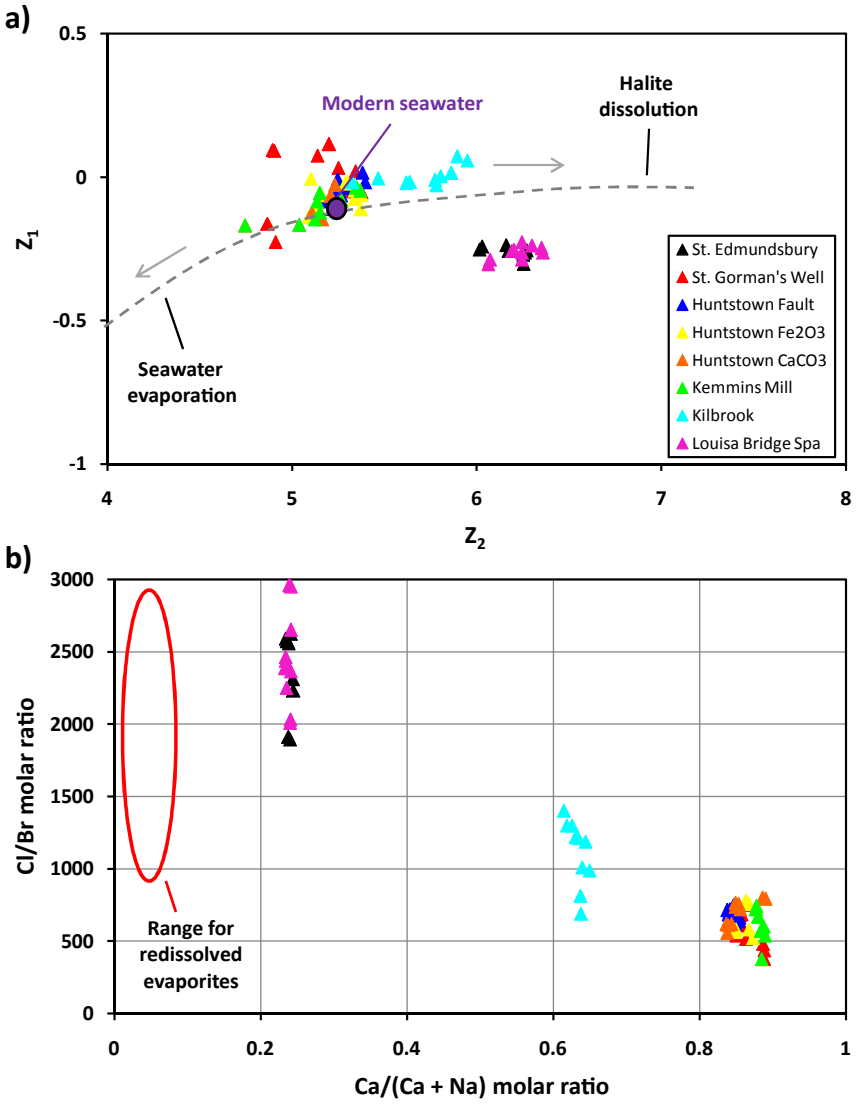

Fig. 8. a) Plot of ilr-coordinates z_1 and z_2 for the Na-Cl-Br system for all thermal spring data. An increase in z_2 due to a lower relative amount of Br suggests the addition of chloride through the dissolution of evaporites (halite). Geochemically modelled pathway for the progressive dissolution of halite by seawater, and modern seawater measurements after Engle and Rowan (2013). b) Relationship between the proportion of Ca to Na in thermal spring waters and the origin of their salinity (as indicated by Cl/Br molar ratios). St. Edmundsbury spring and Louisa Bridge Spa Well lie in the "redissolved evaporites" range of values for Cl/Br (after Yardley and Bodnar, 2014), but contain excess Ca which is probably due to an increased interaction with carbonate bedrock.

and this can be used to assess the degree of evaporite dissolution by the groundwater, as Br is usually excluded from the lattices of evaporite crystals, and is thus depleted in waters that gain their chloride from the dissolution of evaporites. Fig. 8a) shows the ilr-coordinates for the thermal spring data from this study; these data are compared to the geochemically modelled pathway for the progressive dissolution of halite by seawater from Engle and Rowan (2013). Their geochemical model tested the process of halite dissolution versus the evaporation of seawater, and the model assumes no major input of Na, Cl, or Br other than seawater or halite dissolution. Samples containing Na and Cl derived from the evaporation of seawater should plot down and to the left of the value for modern seawater, while meteoric waters which have dissolved halite should plot up and to the right.

The samples from St. Edmundsbury spring and Louisa Bridge Spa Well are distinguished from the other thermal springs as having higher z_2 values, indicating less Br and suggesting that the Cl comes from the dissolution of evaporites (probably halite). The lower values for z_1 for these two springs indicate that the Na/Cl ratio is reduced in these springs. The samples plot below the pathway for halite dissolution but to the right of modern seawater, so the samples from St. Edmundsbury spring and Louisa Bridge Spa Well could represent a mixture between water that dissolved evaporites, and water that has not been accounted for by the simple geochemical model.

Although the use of ratios of raw concentrations has been shown to be problematic (Engle and Rowan, 2013), the Cl/Br mass ratios for the spring waters were examined and compared to existing values in the literature; Cl/Br was found to exceed 200 for Kilbrook spring, St. Edmundsbury spring and Louisa Bridge Spa Well, which suggests that additional chloride is available to the groundwater aside from normal concentrations that may be expected from meteoric recharge and shallow groundwater (Davis et al., 1998; Freeman, 2007). Waters affected by the dissolution of halite commonly have Cl/Br mass ratios of between 1000 and 10,000 (Davis et al., 1998). St. Edmundsbury and Louisa Bridge Spa

springs lie at the lower end of this range (840–1314). The excess chloride is not likely to have an anthropogenic source given that no other common indicators of pollution (such as nitrates or phosphates) were detected in these spring waters, and waters contaminated by sewage generally have lower Cl/Br mass ratios of between 300 and 600 (Davis et al., 1998). The lack of seasonal variation in chloride rules out the application of salt to roads in winter as a source. The origin of the salinity was further investigated by using the relationship between the proportion of Ca to Na in the warm springs and their Cl/Br molar ratios (Fig. 8b)). These results were compared to those for brines from sedimentary basins (Yardley and Bodnar, 2014). St. Edmundsbury spring and Louisa Bridge Spa Well were found to plot in the Cl/Br range for a "redissolved evaporite" source, but to contain higher levels of Ca than redissolved evaporite brines from sedimentary basins (Fig. 8b)). These values of Cl/Br and Ca suggest that these thermal spring waters from the Dublin Basin have derived their excess Cl from the dissolution of an evaporite source, followed by a phase of interaction with carbonate rocks, which has led to an elevated Ca signature compared to the sedimentary basinal brines of Yardley and Bodnar (2014).

The use of both ilr and conventional molar ratios in Fig. 8 strongly suggest that the saline springs have gained their high chloride concentrations from the dissolution of evaporites. Evaporite deposits are not known at present from the vicinity of the Dublin Basin, but they could have precipitated during the deposition of the (basal) terrestrial part of the Devonian sequence, particularly during more arid intervals. For comparison, the Cl/Br mass ratios (345–556) for thermal springs in Bockfjord, Svalbard, Norway (maximum temperature of 25.6 °C) suggest that these springs derived at least part of their excess chloride from evaporitic deposits in Devonian sandstones (Banks et al., 1998). Evaporites could also have formed as a result of fluctuations in sea level during the later Viséan leading to exposure of limestone shelf areas (e.g., Cózar and Somerville, 2005; see also Barham et al., 2012).

Clear evidence to support the existence of either Devonian or Viséan evaporites in or beneath the central Dublin Basin is admittedly lacking. Evaporites are documented in the lower Tournaisian strata of the northwestern part of the Dublin Basin, and on the margins of the Leinster Massif in the southeast of Ireland (Nagy et al., 2005). Dense brines formed by the dissolution of these evaporites could possibly have infiltrated and become trapped in deeper stratigraphic horizons, and these brines may have migrated to the central part of the Dublin Basin. Another potential source for evaporite brines in the Dublin Basin could be the migration of hyper-saline brines from post-Carboniferous evaporite deposits in adjacent offshore basins. In this respect, the halite-dominant facies in the Triassic Mercia Mudstone group of the Kish Bank Basin (e.g., Dunford et al., 2001) could be a possible candidate.

Johnson et al. (2009) investigated the fluids responsible for regional dolomitisation (related to base metal mineralisation) in the Irish Midlands, and included part of the Dublin Basin. From their study of fluid inclusions in minerals, they identified

- a widespread, high-salinity, low-temperature fluid type, which on the basis of enrichment of Cl to Br, they interpreted as being the product of dissolution of halite, and
- elevated levels of K in some of the fluids, which were attributed to interaction with either arkosic Devonian sandstones, or interaction with felsic basement rocks, including the Leinster Granite.

Although the circulation system that emplaced these fluid inclusions was in operation millions of years ago, it is still interesting to note that the hydrochemical results of Johnson et al. (2009) point to dissolution of evaporites and arkosic sandstones, both of which are found within the Devonian sequence of the Irish Midlands.

6.2. C, the "carbonate" link

The carbonate link, ***C***, represents the influence of carbonate bedrock dissolution on the groundwater hydrochemistry. All of the thermal springs and cold seepages in the dataset are hosted in carbonate bedrock, yet some are more heavily influenced by carbonate dissolution than others. Fig. 6a) shows a general division between HCO_3 and Si at one end of the ***C*** link, and SO_4 at the other, representing a trade-off between $HCO_3$and SO_4 in their relationships with Ca. The samples that are closely associated with link ***C*** are distributed so that samples from St. Gorman's Well and Kemmins Mill springs have a greater association with HCO_3, and samples from Huntstown Fault warm spring and the two nearby cold seepages ("Fe_2O_3" and "$CaCO_3$") have a greater association with SO_4.

The addition of sulfate ions to the groundwater may be due to the oxidation of sulfides, such as pyrite (FeS_2). Pyrite is widely present in many lithostratigraphic units in the Dublin Basin. Oxidation of pyrite by the introduction of water in an oxidising environment proceeds as follows:

$$2FeS_2 + 2H_2O + 7O_2 \rightarrow 2FeSO_4 + 2H_2SO_4. \quad (8)$$

The iron sulfate (Fe_2SO_4) can then be converted to ferric iron oxide (Fe_2O_3) in the presence of bacteria (Sutton et al., 2013). The sulfuric acid produced then dissolves the calcium carbonate in the limestone to produce secondary gypsum ($CaSO_4 \cdot 2H_2O$):

$$H_2SO_4 + CaCO_3 \rightarrow CaSO_4 + CO_2 + H_2O. \quad (9)$$

The increased SO_4 in the groundwater comes from the dissolution of the secondary gypsum, with some extra Ca also contributed. However, most of the Ca is likely to come from the interaction of groundwater with the carbonate bedrock itself (with the addition of Mg resulting from dissolution of dolomitised limestone). Thus the sulfate end of link ***C*** is best interpreted as representing the influence of the dissolution of pyrite-hosting carbonates, and in particular, those limestone formations within the Dublin Basin that contain widespread disseminated and vein pyrite. This is a shallow process requiring well-oxygenated input fluids.

The samples closest to the sulfate end of link ***C*** are from the two cold seepages from Huntstown, which have concentrations of Mg and Ca that increase linearly with SO_4. This suggests a similar source for both of these groundwaters, even though their physical appearances are very different (the "Fe_2O_3" seepage is characterised by a conspicuous iron-oxide staining whereas the "$CaCO_3$" seepage is so-called because of its tufa-like deposits). Pyrite is evident in bedrock sampled near to the seepages, so it is highly likely that the SO_4 comes from the dissolution of secondary gypsum caused by the oxidation of pyrite and dissolution of carbonate. However, Fe occurs above the LOQ in only one of these seepages, "Fe_2O_3". The levels of Fe in this seepage vary considerably throughout the year (from 97 ppb in January 2014 to 3494 ppb in August 2014) with the largest values occurring in October 2013 (2198 ppb) and August 2014 (3494 ppb) after two episodes of heavy rainfall. This indicates a strong connection and rapid response to recharge inputs, and suggests that there is a short-term increase in pyrite oxidation after periods of intense recharge. It is possible that the "Fe_2O_3" and "$CaCO_3$" seepages are hydraulically connected, as they both issue from the same lithological horizon.

Springs that are most closely associated with HCO_3 and Si, at the other end of the ***C*** link, include St. Gorman's Well and Kemmins Mill spring. Both of these springs are thermal and have a close

(proximal) association with Waulsortian limestones. The relative enrichment in HCO_3 may be a result of dissolution of the relatively pure carbonate belonging to this particular facies, whereas the relative enrichment in Si may be the result of dissolution of the off-bank, chert-rich limestones and shales.

6.3. M, the "mineralisation" link

The mineralisation link, ***M***, represents the effect of the dissolution of minerals on the hydrochemistry, particularly metal sulfides and oxides. As a process, ***M*** is apparently independent of ***S*** and ***C*** but less important in terms of controlling the overall hydrochemistry of the samples. It controls the minor and trace element hydrochemistry, specifically the metals Mn, Co and Ba. However, ***M*** can also be considered as representing other metals not included in the final dataset, such as Fe; there were too many observations with Fe below the LOQ to include it as a variable in the final MSA. Those samples with a high association with the Mn end of link ***M*** generally have higher Fe too. This is not surprising, as Mn and Fe commonly occur together in hydrothermal mineral deposits in carbonate host rocks (e.g., Wilkinson et al., 2011; Fusswinkel et al., 2014).

As mentioned previously, hydrothermal base metal (Pb-Zn) mineral deposits are a significant feature of the Carboniferous limestones in the Irish Midlands (Fig. 1a)). Barite is commonly associated with these deposits (e.g., Tynagh mine, Co. Galway) and dissolution of this mineral phase could be a contributor of Ba to groundwater. The clr-variance of Ba represents a rather small proportion of the total clr-variance of the dataset (under 2%), so any interpretation regarding Ba is tentative at best. Kilbrook spring has an association with the Ba end of link ***M***, perhaps indicating a relative abundance in Ba from the dissolution of barite in the source aquifer beneath Kilbrook.

The springs with the closest association to the Mn end of link ***M*** are Huntstown "Fe_2O_3" cold seepage and Huntstown Fault thermal spring. These springs have consistently high Mn concentrations and Huntstown Fault spring is the only sampling point in the survey area to consistently show Pb concentrations above the LOQ. Huntstown Fault spring also has the highest Zn levels with concentrations one order of magnitude higher than samples from any other sampling point. Manganese ore could feasibly occur in the same stratigraphic horizons as the Pb-Zn mineral deposits, and was historically mined in the Dublin Basin, in Sutton (Cole, 1922). Huntstown Fault spring discharges from a large Cenozoic strike-slip fault (Moore and Walsh, 2013) in sub-Waulsortian, argillaceous bioclastic strata. Mineralisation is commonly hosted towards the top of these argillaceous bioclastic strata. Given the stratigraphic position of the Huntstown Fault spring, and its proximity to another significant fault of Carboniferous age (Moore and Walsh, 2013), it is possible that the fault from which it springs, or some connecting fault, contains some Pb-Zn mineralisation along its length that is being re-mobilised (dissolved) by the slightly warm water (15.5 °C on average). Samples from the end of the low-recharge period from St. Gorman's Well also lie close to the Mn end of link ***M***, indicating a relative enrichment in Mn that is possibly due to the dissolution of Mn-bearing minerals during this period.

6.4. Temporal variations of the spring waters

The discharge, temperature and hydrochemistry of the thermal springs vary throughout the year. MSA can include many variables and so capture subtle temporal changes in hydrochemistry that may be missed by more traditional techniques (e.g., Helena et al., 2000; King et al., 2014). The PCA biplots (Fig. 6) show the PCA sample scores are most tightly grouped for St. Edmundsbury spring, indicating little annual variation in hydrochemistry. The sample scores for St. Gorman's Well consistently show the greatest dispersion, indicating the highest annual variation in hydrochemistry. This is an expected result as these springs show the least and the greatest annual variations in temperature – ignoring the obvious flooding by river water of St. Edmundsbury spring (see minimum values in Table 3 – the water is released periodically from a dam further upstream).

S reflects the influence of increased water-rock interaction on groundwater hydrochemistry, particularly for St. Edmundsbury spring and Louisa Bridge Spa Well. The implication that these particular springs have longer residence times is further supported by the stable temperature measurements made at both locations. The tight clustering of PCA sample scores from St. Edmundsbury spring suggests little seasonal variability in the spring, and this is supported by the steady temperature profile in Fig. 3a). Apart from the effects of flooding on St. Edmundsbury spring, the temperature remains relatively constant throughout the year (~16 °C). This steady temperature implies that St. Edmundsbury spring is not periodically influenced by shallow, cool, groundwater recharge processes; therefore the warm spring waters must have a longer residence time and a deeper circulation pattern that is insulated from surface and near-surface processes. Louisa Bridge Spa Well (Fig. 3c) behaves slightly differently; the water temperature between April and September is relatively stable (~17 °C), but there is greater variation in temperature between October and April, which is when groundwater recharge is greatest and groundwater levels are highest. It appears that this spring is influenced by mixing with cooler recharge waters during the winter (corroborated by greater dispersion of the PCA sample scores). The stable temperatures recorded during the low recharge period (April to October) suggest a more direct connection at this time between Louisa Bridge Spa Well and the thermal source aquifer.

The observed seasonal differences between Louisa Bridge Spa Well and St. Edmundsbury spring are probably due to differences in their geological settings. Louisa Bridge Spa Well issues from a gravelly till deposit and was discovered in 1794 during the construction of the Royal Canal (Aldwell and Burdon, 1980). Depth to the limestone bedrock is 8.6 m at the site (data from the GSI). This layer of unconsolidated Quaternary overburden may provide a mixing zone for the warm waters to become diluted by shallow, cooler waters in winter. In contrast, St. Edmundsbury spring issues directly from a fissure in the limestone bedrock on the banks of the River Liffey.

St. Gorman's Well has a very complex temperature and EC profile (Fig. 3b), which is suggestive of a non-linear response to recharge, and of turbulent, conduit flow in karstic apertures. The spring has its natural expression as an ephemeral pond, so measurements and samples were collected from a borehole next to the spring. The discharge of the borehole becomes artesian in winter when the pond fills and the temperature of the water increases very rapidly from cold (<11 °C) to a maximum of 21.8 °C. When the flow is not artesian, semi-diurnal fluctuations in water level (Burdon, 1983), temperature and EC (this work) are attributed to the influence of earth tides upon the confined or semi-confined bedrock aquifer (inset in Fig. 3b).

The PCA sample scores for St. Gorman's Well have the largest dispersion in Fig. 6, and the spring appears to be relatively enriched in Si and HCO_3. In Fig. 6b) the hydrochemistry of St. Gorman's Well varies along link ***M***, with warmer samples from the winter recharge period (seasons "c" and "d") showing the least influence from the dissolution of metal-oxides. Samples from the low-recharge period (seasons "a", "b" and "e") show a stronger association with the Mn end of link ***M***, and a higher dissolved metal content. This seasonal difference suggests that the winter thermal water system has a

different and less evolved hydrochemistry than the mid-temperature summer water system. This hydrochemical difference is corroborated by lower EC measurements for the winter flow system (Fig. 3b)), which suggest greater dilution with fresh recharge waters in winter. The seasonal differences in hydrochemistry support the hypothesis that the influx of cooler recharge waters to the karstic flow system in winter facilitates the operation of a relatively deep circulation pattern within the limestone succession which allows cool water to infiltrate quickly to depth, become heated and mixed, and then rapidly ascend to the surface where it issues with a temperature in excess of 20 °C.

7. Conclusion

This study has demonstrated the usefulness of the application of MSA within the CoDa framework in order to better understand the underlying controlling processes governing the hydrochemistry of a group of thermal springs in a low-enthalpy setting, each with different geological and hydrogeological settings, and with distinctive and differing patterns of annual behaviour.

Assessment of major ion data (Fig. 6a) clearly suggests two distinct independent processes controlling the hydrochemistry of the thermal springs dataset. The "water-rock interaction" link, ***S***, represents the influence of increased water-rock-interaction processes and demonstrates that the springs associated with the Na/Cl end of the link are not typical Ca–HCO_3-type groundwaters, which would normally be expected in a limestone aquifer such as the Carboniferous bedrock of the Dublin Basin. The "carbonate" link, ***C***, represents the effect of the dissolution of different types of limestone bedrock on the hydrochemistry (simplified as a trade-off between SO_4 and HCO_3). The inclusion of all available data for the thermal springs (30 variables) into the PCA identified a third distinct process controlling the hydrochemistry (Fig. 6b)). The "mineralisation" link, ***M***, represents the influence of the dissolution of mineral deposits associated with the carbonate bedrock, particularly Mn at one end of the link, and Ba at the other. This process is less important in the control of the overall hydrochemistry as it affects only minor and trace ions, and metals in particular.

Springs associated with the Na/Cl end of link ***S*** are likely to have a moderate to high temperature with very little annual variation. They are characterised by higher salinity and EC due to an increased water-rock-interaction and residence time. The source aquifer is likely to be deep, confined and well-insulated from fluctuating near-surface hydrogeological processes. The excess Na and Cl observed in these springs are not due to any anthropogenic contamination but instead possibly derive from the dissolution of evaporites. The precise origin of the evaporites required to facilitate this process remains cryptic at present, and the source lithology may be either intra- or extra-basinal. The hydrochemistry of St. Edmundsbury spring and Louisa Bridge Spa Well is closely associated with the Na/Cl end of link ***S***; they appear to be fed from the same aquifer (or two very similar aquifers), and must have their source beneath the carbonate Dublin Basin, perhaps within the Devonian terrestrial strata.

Springs with a closer association to link ***C*** rather than link ***S*** are likely to be cold, or cooler thermal springs (with the exception of St. Gorman's Well, which has extremely variable moderate to high temperatures). Depending upon their location along link ***C***, they can be relatively enriched in either SO_4, probably controlled by the oxidation of sulfides such as pyrite, or relatively enriched in HCO_3 and Si, probably controlled by the dissolution of pure Waulsortian limestones and associated chert layers. They are likely to have an unconfined or semi-confined source and a good supply of fresh, infiltrating, recharge waters. It is likely that the source is a relatively shallow one, as oxidising waters are required for both pyrite and carbonate dissolution.

Springs associated with the Mn end of link ***M*** are also likely to be associated with high Fe content and dissolution of pyrites hosted in the carbonate bedrock. These springs are most similar to cold groundwater from the shallow bedrock boreholes at Ryewater in terms of their major ion hydrochemistry.

The compositional MSA has greatly facilitated the investigation of a large hydrochemical dataset and has highlighted the influence of at least two different aquifer types (one deep, one shallow) on several of the Irish thermal springs examined. The results of the compositional MSA also facilitate assessment of the temporal variations in the hydrochemistry of the thermal springs, and have provided an insight into the seasonal variations of St. Gorman's Well, where the complex temperature and EC profiles of this spring are due to conduit flow within karstified bedrock.

Acknowledgements

This work was carried out as part of the IRETHERM project, which is funded by Science Foundation Ireland (grant number 10/IN.1/I3022), in collaboration with the IRETHERM team (www.iretherm.ie). We acknowledge the Hydrometric and Groundwater Section of the Environmental Protection Agency, for providing the water analyses for the Ryewater boreholes from the Water Framework Directive groundwater monitoring programme. Figures were produced with the help of free software from USGS and the R community, particularly the R package "ggbiplot". We would also like to thank Cora McKenna, Dr. Liam Morrison, interns, staff and students at DIAS who helped with data acquisition, and various landowners and tenants for granting us access to the springs. Thanks to John Paul Moore of UCD for helpful comments on early versions of the manuscript. We gratefully thank our reviewers, Dr. Mark Engle and another anonymous reviewer, for their constructive comments.

Appendix A. Supplementary data

Supplementary data related to this article can be found at http://dx.doi.org/10.1016/j.apgeochem.2016.05.008.

References

Aitchison, J., 1986. The Statistical Analysis of Compositional Data. Chapman and Hall Ltd., London.
Aitchison, J., Greenacre, M., 2002. Biplots of compositional data. Appl. Stat. 51, 375–392.
Aitchison, J., Barceló-Vidal, C., Martín-Fernández, J.A., Pawlowsky-Glahn, V., 2000. Logratio analysis and compositional distance. Math. Geol. 32, 271–275.
Aldwell, C.R., Burdon, D.J., 1980. Hydrogeothermal Conditions in Ireland. XXVI International Geological Congress. Fossil Fuels Sec, Paris, 14.2; 14.0068:21.
Aquilina, L., Pauwels, H., Genter, A., Fouillac, C., 1997. Water-rock interaction process in the Triassic sandstone and granitic basement of the Rhine Graben: geochemical investigation of a geothermal reservoir. Geochim. Cosmochim. Acta 61, 4281–4295.
Banks, D., Sletten, R.S., Haldorsen, S., Dale, B., Heim, M., Swensen, B., 1998. The thermal springs of Bockfjord, Svalbard: occurrence and major ion hydrochemistry. Geothermics 27, 445–467.
Barham, M., Murray, J., Joachimski, M.M., Williams, D.M., 2012. The onset of the Permo-Carboniferous glaciation: reconciling global stratigraphic evidence with biogenic apatite $\delta^{18}O$ records in the late Visean. J. Geol. Soc. 169, 119–122.
Boyce, A.J., Little, C.J., Russell, M.J., 2003. A new fossil vent biota in the Ballynoe barite deposit, Silvermines, Ireland: evidence for intracratonic sea-floor hydrothermal activity about 352 Ma. Econ. Geol. 98, 649–656.
Buccianti, A., Grunsky, E., 2014. Compositional data analysis in geochemistry: are we sure to see what really occurs during natural processes? J. Geochem. Explor. 141, 1–5.
Buccianti, A., Nisi, B., Martín-Fernández, J.A., Palarea-Albaladejo, J., 2014. Methods to investigate the geochemistry of groundwaters with values for nitrogen compounds below the detection limit. J. Geochem. Explor. 141, 78–88.
Burdon, D.J., 1983. Irish Geothermal Project, Phase 1. Geological Survey of Ireland,

Dublin. Report 150/75/15.
Busby, J., 2010. Geothermal prospects in the United Kingdom. In: Proceedings World Geothermal Congress 2010, Bali, Indonesia.
Castillo, C., Azaroual, M., Ignatiadis, I., Goyénèche, O., 2011. Geochemical parameters as precursors to predict the decline of temperature in the Dogger Aquifer (Paris Basin, France). In: Proceedings of Thirty-sixth Workshop on Geothermal Reservoir Engineering, Stanford University, California. SGP-TR-191.
Chew, D.M., 2012. The Grampian evolution of the Caledonides of NW Ireland. Open Univ. Geol. Soc. J. 33 (1), 19–25.
Cloutier, V., Lefebvre, R., Therrien, R., Savard, M.M., 2008. Multivariate statistical analysis of geochemical data as indicative of the hydrogeochemical evolution of groundwater in a sedimentary rock aquifer system. J. Hydrol. 353, 294–313.
Cole, G.A.J., 1922. Memoir and map of localities of minerals of economic importance and metalliferous mines in Ireland. Mem. Geol. Surv. Irel. 155.
Cózar, P., Somerville, I.D., 2005. Stratigraphy of upper Viséan carbonate platform rocks in the Carlow area, southeast Ireland. Geol. J. 40, 35–64.
Daughney, C.J., Raiber, M., Moreau-Fournier, M., Morgenstern, U., van der Raaij, R., 2012. Use of hierarchical cluster analysis to assess the representativeness of a baseline groundwater quality monitoring network: comparison of New Zealand's national and regional groundwater monitoring programs. Hydrogeol. J. 20, 185–200.
Davis, J.C., 1986. Statistics and Data Analysis in Geology. John Wiley & Sons Inc., New York.
Davis, S.N., Whittemore, D.O., Fabryka-Martin, J., 1998. Uses of chloride/bromide ratios in studies of potable water. Groundwater 36, 338–350.
Davis, S.N., Cecil, L.D., Zreda, M., Moysey, S., 2001. Chlorine-36, bromide, and the origin of spring water. Chem. Geol. 179, 3–16.
Drew, L.J., Grunsky, E.C., Scheunemeyer, J.H., 2008. Investigation of the structure of geological process through multivariate statistical analysis – the creation of a coal. Math. Geosci. 40, 789–811.
Dunford, G.M., Dancer, P.N., Long, K.D., 2001. Hydrocarbon potential of the Kish Bank basin: integration within a regional model for the greater Irish Sea Basin. In: Shannon, P.M., Haughton, P.D.W., Corcoran, D.V. (Eds.), The Petroleum Exploration of Ireland's Offshore Basins, vol. 188. Geological Society, London, pp. 135–154. Special Publication.
Edmunds, W.M., Guendouz, A.H., Mamou, A., Moulla, A., Shand, P., Zouari, K., 2003. Groundwater evolution in the Continental Intercalaire aquifer of southern Algeria and Tunisia: trace element and isotope indicators. Appl. Geochem. 18, 805–822.
Edmunds, W.M., Smedley, P.L., 2000. Residence time indicators in groundwater: the East Midlands Triassic sandstone aquifer. Appl. Geochem. 15, 737–752.
Egozcue, J.J., Pawlowsky-Glahn, V., Mateu-Figueras, G., Barceló-Vidal, C., 2003. Isometric logratio transformations for compositional data analysis. Math. Geol. 35, 279–300.
Engle, M.A., Blondes, M.S., 2014. Linking compositional data analysis with thermodynamic geochemical modelling: oilfield brines from the Permian Basin, USA. J. Geochem. Explor. 141, 61–70.
Engle, M.A., Rowan, E.L., 2013. Interpretation of Na–Cl–Br systematics in sedimentary basin brines: comparison of concentration, element ratio, and isometric log-ratio approaches. Math. Geosci. 45, 87–101.
Engle, M.A., Rowan, E.L., 2014. Geochemical evolution of produced waters from hydraulic fracturing of the Marcellus Shale, northern Appalachian Basin: a multivariate compositional data analysis approach. Int. J. Coal Geol. 126, 45–56.
Engle, M.A., Gallo, M., Schroeder, K.T., Geboy, N.J., Zupancic, J.W., 2014. Three-way compositional analysis of water quality monitoring data. Environ. Ecol. Stat. 21, 565–581.
Fallon, P., Murray, J., 2015. Conodont biostratigraphy of the mid-Carboniferous boundary in Western Ireland. Geol. Mag. http://dx.doi.org/10.1017/S0016756815000072.
Filzmoser, P., Hron, K., Reimann, C., 2009a. Univariate statistical analysis of environmental (compositional) data: problems and possibilities. Sci. Total Environ. 407, 6100–6108.
Filzmoser, P., Hron, K., Reimann, C., 2009b. Principal component analysis for compositional data with outliers. Environmetrics 20, 621–632.
Freeman, J.T., 2007. The use of bromide and chloride mass ratios to differentiate salt-dissolution and formation brines in shallow groundwaters of the Western Canadian Sedimentary Basin. Hydrogeol. J. 15, 1377–1385.
Freeze, R.A., Cherry, J.A., 1979. Groundwater. Prentice Hall, New Jersey.
Fusswinkel, T., Wagner, T., Wenzel, T., Wälle, M., Lorenz, J., 2014. Red bed and basement sourced fluids recorded in hydrothermal Mn-Fe-As veins, Sailauf (Germany): a LA-ICPMS fluid inclusion study. Chem. Geol. 363, 22–39.
Gabriel, K.R., 1971. The biplot-graphic display of matrices with application to principal component analysis. Biometrika 58, 453–467.
Giménez-Forcada, E., Vega-Alegre, M., 2015. Arsenic, barium, strontium and uranium geochemistry and their utility as tracers to characterize groundwaters from the Espadán-Calderona Triassic Domain, Spain. Sci. Total Environ. 512–513, 599–612.
Goodman, R., Jones, G., Kelly, J., Slowey, E., O'Neill, N., 2004. Geothermal Energy Resource Map of Ireland Final Report. Sustainable Energy Ireland (SEI), Dublin.
Graham, J.R., 2009. Devonian. In: Holland, C.H., Sanders, I.S. (Eds.), The Geology of Ireland, second ed. Dunedin Academic Press Ltd, Edinburgh, pp. 175–214.
Güler, C., Thyne, G.D., McCray, J.E., Turner, A.K., 2002. Evaluation of graphical and multivariate statistical methods for classification of groundwater chemistry. Hydrogeol. J. 10, 455–474.
Güler, C., Kurt, M.A., Alpaslan, M., Akbulut, C., 2012. Assessment of the impact of anthropogenic activities on the groundwater hydrology and chemistry in Tarsus coastal plain (Mersin, SE Turkey) using fuzzy clustering, multivariate statistics and GIS techniques. J. Hydrol. 414–415, 435–451.
Helena, B., Pardo, R., Vega, M., Barrado, E., Fernandez, J.M., Fernandez, L., 2000. Temporal evolution of groundwater composition in an alluvial aquifer (Pisuerga River, Spain) by principal component analysis. Water Resour. 34 (3), 807–816.
Henry, T., 2014. An Integrated Approach to Characterising the Hydrogeology of the Tynagh Mine Catchment, County Galway, Ireland. Ph.D. thesis. National University of Ireland Galway (unpublished).
Hu, S., Luo, T., Jing, C., 2013. Principal component analysis of fluoride geochemistry of groundwater in Shanxi and Inner Mongolia, China. J. Geochem. Explor. 135, 124–129.
Hunter Williams, N., Misstear, B., Daly, D., Johnston, P., Lee, M., Cooney, P., Hickey, C., 2011. A national groundwater recharge map for Ireland. In: Proceedings National Hydrology Conference, Irish National Committees for the IHP and ICID, pp. 89–109.
Johnson, A.W., Shelton, K.L., Gregg, J.M., Somerville, I.D., Wright, W.R., Nagy, Z.R., 2009. Regional studies of dolomites and their included fluids: recognizing multiple chemically distinct fluids during the complex diagenetic history of Lower Carboniferous (Mississippian) rocks of the Irish Zn-Pb ore field. Mineral. Petrol. 96 (1–2), 1–18.
King, A.C., Raiber, M., Cox, M.E., 2014. Multivariate statistical analysis of hydrochemical data to assess alluvial aquifer-stream connectivity during drought and flood: Cressbrook Creek, southeast Queensland, Australia. Hydrogeol. J. 22, 481–500.
Krešić, N., 2007. Hydrogeology and Groundwater Modelling, second ed. CRC Press, Boca Raton, Florida.
Lees, A., Miller, J., 1995. Waulsortian banks. In: Monty, C.L.V., Bosence, D.W.J., Bridges, P.H., Pratt, B.R. (Eds.), Carbonate Mud-mounds: Their Origin and Evolution. Special Publication of the International Association of Sedimentologists, vol. 23. Blackwell Science, Oxford, pp. 191–271.
MacDermot, C.V., Sevastopulo, G.D., 1972. Upper Devonian and lower Carboniferous stratigraphical setting of Irish mineralisation. Geol. Surv. Irel. Bull. 1, 267–280.
Marchant, T.R., Sevastopulo, G.D., 1980. The Calp of the Dublin district. J. Earth Sci. R. Dublin Soc. 5, 195–203.
Menció, A., Folch, A., Mas-Pla, J., 2012. Identifying key parameters to differentiate groundwater flow systems using multifactorial analysis. J. Hydrol. 472–473, 301–313.
Mooney, B., Allen, A., Koniger, P., 2010. Investigation of source and conduit for warm geothermal waters, North Cork, Republic of Ireland. In: Proceedings World Geothermal Conference, Bali, Indonesia.
Moore, J.P., Walsh, J.J., 2013. Analysis of fracture systems and their impact on flow pathways in Irish bedrock aquifers. Geol. Surv. Irel. Groundw. Newsl. 51, 28–33.
Nagy, Z.R., Somerville, I.D., Gregg, J.M., Becker, S.P., Shelton, K.L., 2005. Lower Carboniferous peritidal carbonates and associated evaporites adjacent to the Leinster Massif, southeast Irish Midlands. Geol. J. 40, 173–192.
Otero, N., Tolosana-Delgado, R., Soler, A., Pawlowsky-Glahn, V., Canals, A., 2005. Relative vs. Absolute statistical analysis of compositions: a comparative study of surface waters of a Mediterranean river. Water Res. 39, 1404–1414.
Page, R.M., Lischeid, G., Epting, J., Huggenberger, P., 2012. Principal component analysis of time series for identifying indicator variables for riverine groundwater extraction management. J. Hydrol. 432–433, 137–144.
Palarea-Albaladejo, J., Martín-Fernández, J.A., 2008. A modified EM alr-algorithm for replacing rounded zeros in compositional data sets. Comput. Geosci. 34, 902–917.
Palarea-Albaladejo, J., Martín-Fernández, J.A., 2015. zCompositions – R package for multivariate imputation of left-censored data under a compositional approach. Chemom. Intell. Lab. Syst. 143, 85–96.
Palarea-Albaladejo, J., Martín-Fernández, J.A., Buccianti, A., 2014. Compositional methods for estimating elemental concentrations below the limit of detection in practise using R. J. Geochem. Explor. 141, 71–77.
Parkhurst, D.L., Appelo, C.A.J., 1999. User's Guide to PHREEQC (Version 2) – a Computer Program for Speciation, Batch-reaction, One-dimensional Transport, and Inverse Geochemical Calculations. U.S. Geological Survey Water-Resources Investigations Report 99–4259.
Pavlovskiy, I., Selle, B., 2015. Integrating hydrogeochemical, hydrogeological, and environmental tracer data to understand groundwater flow for a karstified aquifer system. Groundwater 53, 156–165.
R Development Core Team, 2015. R: a Language and Environment for Statistical Computing. R Foundation for Statistical Computing, Vienna. http://www.R-project.org/.
Raiber, M., White, P.A., Daughney, C.J., Tschritter, C., Davidson, P., Bainbridge, S.E., 2012. Three-dimensional geological modelling and multivariate statistical analysis of water chemistry data to analyse and visualise aquifer structure and groundwater composition in the Wairau Plain, Marlborough District, New Zealand. J. Hydrol. 436–437, 13–34.
Reyes, A.G., Trompetter, W.J., 2012. Hydrothermal water-rock interaction and the redistribution of Li, B and Cl in the Taupo Volcanic Zone, New Zealand. Chem. Geol. 314–317, 96–112.
Sevastopulo, G.D., Wyse Jackson, P.N., 2009. Carboniferous (Dinantian). In: Holland, C.H., Sanders, I.S. (Eds.), .The Geology of Ireland, second ed. Dunedin Academic Press Ltd, Edinburgh, pp. 241–288.
Somerville, I.D., 2008. Biostratigraphic zonation and correlation of Mississippian rocks in Western Europe: some case studies in the lateViséan/Serpukhovian. Geol. J. 43, 209–240.

Sparacino, M., Camussi, M., Colombo, M., Carella, R., Sommaruga, C., 2007. The world's largest geothermal district heating using ground water under construction in Milan (Italy)-AEM unified heat pump project. In: Proceedings of the European Geothermal Congress, Unterhaching, Germany, vol. 30.

Strogen, P., Somerville, I.D., Pickard, N.A.H., Jones, G.L.L., Fleming, M., 1996. Controls on ramp, platform and basinal sedimentation in the Dinantian of the Dublin Basin and Shannon trough, Ireland. In: Strogen, P., Somerville, I.D., Jones, G.L.L. (Eds.), Recent Advances in Lower Carboniferous Geology, vol. 107. Geological Society, London, pp. 263–279. Special Publication.

Sutton, D., McCabe, B., O'Connell, A., Cripps, J., 2013. A laboratory study of the expansion of a pyritic mudstone/siltstone fill material. Eng. Geol. 152, 194–201.

Tanasković, I., Golobocanin, D., Miljević, N., 2012. Multivariate statistical analysis of hydrochemical and radiological data of Serbian spa waters. J. Geochem. Explor. 112, 226–234.

Van den Boogaart, K.G., Tolosana-Delgado, R., 2008. "compositions": a unified R package to analyze compositional data. Comput. Geosci. 34 (4), 320–338.

Van den Boogaart, K.G., Tolosana-Delgado, R., 2013. Analyzing Compositional Data with R. Springer-Verlag, Heidelberg.

Walsh, S., 2012. A Summary of Climate Averages 1981–2010 for Ireland. Climatological Note No.14.Met Éireann, Dublin.

Wang, W., Zhao, J., Cheng, Q., 2014. Mapping of Fe mineralization-associated geochemical signatures using logratio transformed stream sediment geochemical data in eastern Tianshan, China. J. Geochem. Explor. 141, 6–14.

Wilkinson, J.J., 2010. A review of fluid inclusion constraints on mineralization in the Irish ore field and implications for the genesis of sediment-hosted Zn-Pb deposits. Econ. Geol. 105, 417–442.

Wilkinson, J.J., Hitzman, M.W., 2015. The Irish Zn-Pb Orefield: the View from 2014. In: Archibald, S.M., Piercey, S.J. (Eds.), Current Perspectives on Zinc Deposits. Irish Association for Economic Geology, Dublin, pp. 59–72.

Wilkinson, J.J., Crowther, H.L., Coles, B.J., 2011. Chemical mass transfer during hydrothermal alteration of carbonates: controls of seafloor subsidence, sedimentation and Zn-Pb mineralization in the Irish Carboniferous. Chem. Geol. 289 (1–2), 55–75.

Yardley, B.W.D., Bodnar, R.J., 2014. Fluids in the continental crust. Geochem. Perspect. 3 (1), 1–123.